Recent Progress on Ligand-Protected Metal Nanoclusters in Photocatalysis

Meegle Mathew, Greeshma Krishnan, Amita Aanne Mathews, Kevin Sunil, Leo Mathew, Rodolphe Antoine, Sabu Thomas

nanomaterials

MDPI

Review

Recent progress on ligand protected metal nanoclusters in photocatalysis

Meegle S Mathew[1a], Amita Aanne Mathews[1], Greeshma Krishnan[1], Kevin Sunil[1], Leo Mathew[1], Rodolphe Antoine[2]* and Sabu Thomas[1]*

[1] School of Energy Materials, Mahatma Gandhi University, Priyadarsini Hills P O, Kottayam-686560 email: meeglesmathew@gmail.com and sabuthomas@mgu.ac.in

[a] Research and PG Department of Chemistry, Mar Athanasius College, Kothamangalam

[2] Institut Lumière Matière UMR 5306, Univ Lyon, Université Claude Bernard Lyon 1, CNRS, F-69100 Villeurbanne, France, email: rodolphe.antoine@univ-lyon1.fr

* Correspondence: rodolphe.antoine@univ-lyon1.fr; sabuthomas@mgu.ac.in

Abstract: The reckless use of non-replenishable fuels by the growing population for energy and the resultant incessant emission of hazardous gases and waste products into the atmosphere insisted that scientists fabricate materials capable of managing these global threats at once. In recent studies, photocatalysis employed focus on utilizing renewable solar energy to initiate chemical processes with the aid of semiconductors and highly selective catalysts. A wide range of nanoparticles has showcased promising photocatalytic properties. Metal nanoclusters (MNCs) with sizes below 2nm, stabilized by ligands, show discrete energy levels and exhibit unique optoelectronic properties, which are vital to photocatalysis. In this review, we intend to compile information on the synthesis, true nature, stability of the MNCs decorated with ligands and varying photocatalytic efficiency of metal NCs concerning changes in the aforementioned domains. The review discusses the photocatalytic activity of atomically precise ligand-protected MNCs and their hybrids in the domain of energy conversion processes like photodegradation of dyes, oxygen evolution reaction (ORR), hydrogen evolution reaction (HER) and CO_2 reduction reaction (CO_2RR)

Keywords: photocatalysis; metal nanoclusters; CO_2 reduction; hydrogen evolution reaction; photodegradation

1. Introduction

Over the past several decades, the rising demands of the ever-growing population, excessive consumption of non-renewable resources, resulting greenhouse gas emissions, and improper waste disposal have greatly concerned humanity. The relentless efforts of the scientific community towards this global crisis paved the way for more sustainable solutions like photocatalysis. Photocatalysis appears to be a perfect fit as a greener alternative to resolve energy and pollution-related problems simultaneously, and it aids the completion of chemical processes with the help of inexhaustible solar power, mitigates hazardous products like CO_2 by photoreduction, and produces cleaner fuels. In 1972, Fujishima and Honda were the first to apply this strategy for hydrogen evolution reaction through photocatalysis [1]. Later, photocatalysis with semiconductors with sufficient bandgaps (i.e., TiO_2, CdS, ZnO, Fe_2O_3, and ZnS) did turn into a promising field of study for researchers [2–6]. Nanotechnology has created revolutionary changes in this dimension with the help of umpteen nanoparticles (NPs) which possess a high surface area and plasmonic resonance. Noble metal nanoparticles such as AuNPs, AgNPs, PtNPs, IrNPs, OsNPs, RhNPs, and RuNPs have been employed mainly for photocatalysis for decades, but the efficiency has not reached the target level [7]. Apart from this, the mechanisms-related information in photocatalysis driven by noble metal NPs with massive surface atoms did seem vague. Meanwhile, a new class of zero-dimensional fluorophores, MNCs, proved dominant to their conventional nanoparticle ana-

Citation: To be added by editorial staff during production.

Academic Editor: Firstname Lastname

Received: date
Revised: date
Accepted: date
Published: date

logs in various applications.

MNCs comprise a core with ten to hundreds of atoms protected by surface ligands like thiols, proteins, peptides, enzymes, polymers, and DNA [8–11]. The emergence of these well-defined aggregates with commendable surface-to-volume ratio, fully reduced atomic core, and dispersity on catalysts made them the best choice for a wide range of applications [12]. Compared to bulk, MNCs being a sub-nanometer-sized unit (< 2nm), exhibits quantum confinement effects as it approaches the Fermi wavelength of conduction electrons, thereby splitting the continuous density of states into discrete energy levels. As a result, MNCs possess molecule-like behavior and act as a missing link between atoms/molecules and metal nanoparticles [13]. The atomic level precision of MNCs assisted in confining size and analyzing involved mechanisms quite understandable. Due to these factors, they have also been assigned a few other titles, such as quantum clusters (QCs) and monolayer protected clusters [14,15]. Initially, gold nanocluster (AuNCs) were the focus of study due to the simple synthetic routes, commendable stability and novel optical properties presented, even in the absence of plasmonic resonance, which are all attributed to their shift in valency from Au (III) to Au (I)/Au(0) in AuNCs [16].

The physicochemical properties of NCs are highly influenced by the size, metal core composition, assembly architecture, and surface components [17–19]. In addition, MNCs are known for their attractive optical characteristics, including tunable luminescence, HOMO–LUMO transitions, substantial Stokes shift, two-photon absorption, photostability, magnetism, chirality and biocompatibility [20,21]. Their photostability, biocompatibility, and low cytotoxicity, in turn, caused them to be chosen for biomedical applications [22]. Monolayer-protected clusters are less aggressive and relatively more stable than gas-phase clusters containing unsatisfied valence electrons in their free state. Currently, further studies on the factors and their impacts on optical properties set forth new developments in catalysis, biosensing, bioimaging, gene therapy, and drug delivery [13,23–26]. Tailoring a cluster's distinctive optical and electronic properties by enhancing parameters like formal charges, geometry, metal composition, and ligand plays a pivotal role in photocatalysis [27]. Despite these, MNCs with fully reduced metal atom cores have relatively low-band gaps, thus inhibiting photo-corrosion appreciably. Therefore, MNCs can be utilized, as photosensitizers and cocatalysts, in energy-intensive processes like the photodegradation of dyes, ORR, HER, and CO_2RR [28–31]. (Figure 1)

A comprehensive review of metal nanomaterials for heterogeneous catalysis has been written by Liu and Corma [12]. Jianping Xie and colleagues highlighted in a minireview the major important characteristics of MNCs, which are vital to photo and electro-catalysis [27]. This review aims to update the literature on MNCs -synthetic routes, physicochemical properties, stability, and recent advances with a focus on photocatalysis, particularly from 2016 onwards, since a comprehensive review on catalytic applications of ligand-protected, atomically precise MNCs was published in Coordination Chemistry Journal in 2016 to which the readers are referred to [32].

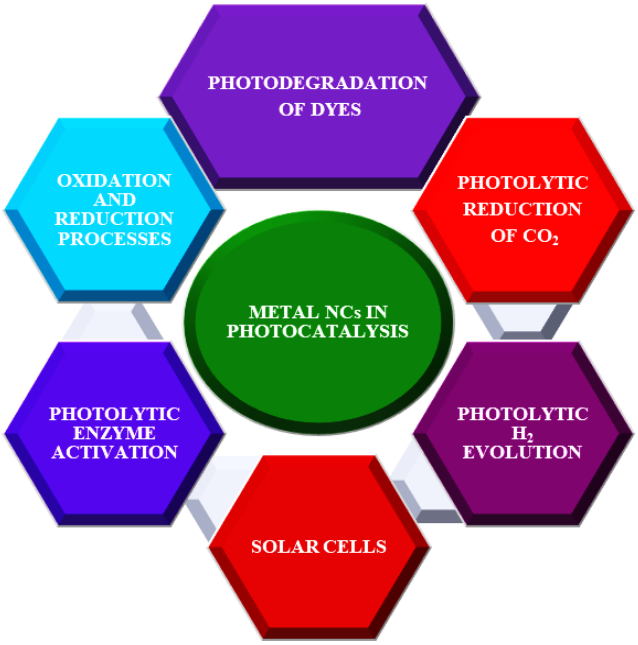

Figure 1. Applications of MNCs in photocatalysis.

2.1. Chemical Composition and structural properties

The central metal atom, ligands, charge states and composition play a significant role in deciding the physicochemical properties of MNCs. In general, MNCs are expressed by the molecular formula $[M_n(SR)_m]^q$ (n- represents the number of metal atoms, m- represents the thiolate ligands (staple motif), and q denotes the net charge of the cluster) [33]. Engineering metal, ligand, and charge state on an atomic level can alter the performances and physicochemical properties of MNCs. In addition, the size (~2nm) and structure can be adjusted with atomic precision for new application possibilities in various disciplines [34]. By analogy with the terminology employed in the protein field, MNCs are composed of primary, secondary, and tertiary structures. Whereas the metallic core is the primary structure, and the repetitive local structural motifs serve as a bridge between the core and the ligands. These motifs are organic ligands, and surprisingly, the length or size, and structure can be easily manipulated, resulting in a wide range of MNCs. The protective shell's exterior structure is made up of spatial ligands. It has been highlighted that insight into the crystal structure of the material is very crucial as it reveals information on the atomicity of the core, the nature of the Au–S linkage, the chirality of the NCs, the arrangements of the ligands around the metal core, and so on [35]. In recent times, crystal structures of some of the AuNCs such as $Au_{102}SR_{44}$, [36] $Au_{25}SR_{18}$, [36] $Au_{38}SR_{24}$, [37] $Au_{36}SR_{24}$, [38] $[Au_{24}(PPh_3)_{10}(SR)_5Cl_2]^+$, [39] $Au_{28}SR_{20}$, [40] (where SR= thiolate) were resolved using various analytical techniques [41].

The molecular weight of MNCs is identified using mass spectrometry-based methods, like matrix-assisted laser-desorption ionization-time of flight mass spectrometry (MALDI-TOF-MS) and electrospray ionization mass spectrometry (ESI-MS) [42,43]. For MALDI analysis, traditional weak organic acids are used as matrices to recognize the molecular mass of the core of the MNCs; Even though it is a sophisticated analytical instrument, it also has some limitations. The weak organic acid matrices employed in MALDI do not eliminate ligand fragmentation. The mass accuracy of MS equipment is also decreased by the presence of significant chemical noise and/or an unresolved isotopic pattern, which leads to the possibility of numerous molecular formulae being nearly isobaric and the potential for impurities or ligand fragmentation to produce significant chemical noise that makes it difficult to assign atomic information. For instance, isotope-resolved mass spectrometry has been pushed forwards by Antoine's group to unravel the molecular formula of ultrasmall NCs [44].

2.2 Synthesis of Metal Nanocluster

2.2.1 General Synthetic Methods

A uniform, monodisperse catalyst with a known structure and composition should be desirable for the development of an effective catalyst. There are several synthetic techniques that can be used to produce luminescent metal nanoclusters with various sizes, structures, and surface characteristics. The conventional methods to produce these luminescent metal nanoclusters are various template methods, the photoreduction method, the sonochemical method, the microemulsion method, the radiolytic method, the electrochemical method, microwave assisted synthesis seed growth method, monolayer-protected method, phase transfer synthesis, etching method etc,. In general, the nanocluster synthesis can be categorized as a top-down approach, bottom-up approach and inter-cluster conversion approach [45].

2.2.2 Bottom-up Method

The bottom-up method uses metal salt, ligands and reducing agents as precursors. In this method, nanoclusters are formed by wet chemical reduction of metal salts with a suitable reducing agent. In the first stage, a metal(I)-thiolate complex is formed by reacting metal salt with thiolate ligand. Then, metal(I)-thiolate complex is treated with a reducing agent such as sodium borohydride ($NaBH_4$) or ascorbic acid to reduce M(I) to M(0) and produce M(0)@M(I)-based NCs [46]. This method of synthesis is also known as one-step synthesis. Nigeshi *et al*. synthesized and isolated a series of nanoclusters with different compositions ($Au_{10}(SG)_{10}$, $Au_{15}(SG)_{13}$, $Au_{18}(SG)_{14}$, $Au_{22}(SG)_{16}$, $Au_{22}(SG)_{17}$, $Au_{25}(SG)_{18}$, $Au_{29}(SG)_{20}$, $Au_{33}(SG)_{22}$, and $Au_{39}(SG)_{24}$) using glutathione (SG) as stabilizing agent [47].

In some circumstances, the stabilizing ligand itself serves as a reducing agent, which eliminates the need for a second reducing agent. This technique of synthesis is known as the biomineralization method [48]. Other than wet chemical reduction, the photoreduction method is also employed to produce luminescent metal nanoclusters, which initiate the reduction reaction in light. Zhou *et al*. employed a photoreduction method for the synthesis of AuNCs stabilized by silane. The silane-stabilized nanocluster was further used for the photodegradation of an organic dye methene blue [49].

2.2.3 Top-down Method

In the top-down approach, ultra-smaller-sized MNCs can be prepared from larger-sized metal nanoparticles/MNCs via chemical etching. Here, chemical etching is carried out between excess ligands and larger metal nanoclusters to obtain metal NCs with smaller sizes. This is usually done in the solution phase, either in one solution or in the interface of two solutions. Based on the use of an etching agent, the etching method is classified into two categories, ligand etching and solvent etching. One major advantage of nanoclusters produced by the etching method is the controlled size focusing [50]. This method not only provides monodisperse metal nanocluster but also give alloy nanocluster [51,52].

2.2.4 Inter-cluster conversion method

In the inter-cluster conversion method, the NCs formed via seed-mediated synthesis, cluster conversion, metal exchange ligand exchange, and motif exchange. In this process, nanoclusters are used as the starting material, and the structure of the nanoclusters is changed through the adjustment of kinetic or thermodynamic parameters. The most common method for cluster conversion is the ligand exchange reaction (LER) [53]. LER is a widely used technique for modifying nanoclusters after their creation. The adaptability of the gold and sulfur interphase makes this possible. The ability to change the size and phase of clusters and impart fluorescence on nanoclusters for biological labelling purposes, are some advantages of LER. They can also increase the enantiomeric excess of already chiral clusters and give chirality to nonchiral clusters. In this way, LER broadens the range of MNCs by forming distinctive and precise nanoclusters [54]. Wang and co-worker summarise the various LER on thiolate-protected gold nanoclusters and their advantages [54–56].

Bootharaju *et al*. developed a procedure for reversible transformation of NCs with different size. A reversible transformation of $[Ag_{35}(SG)_{18}$ to $Ag_{44}(4\text{-FTP})_{30}]$ or shrinkage of $[Ag_{44}(4\text{-FTP})_{30}$ to $Ag_{35}(SG)_{18}]$ were carried out using the ligand SG and 4-fluorothiophenol (4-FTP) [57]. Similarly, an electrochemical method for crystallization of NCs were put forward by Antonollo *et al.* [58]. Using

this method a large quantity of high-quality crystalline $Au_{25}(SR)_{18}$ NCs can be obtained. This method of crystallization can aid in determining the structure of new NCs, enabling a deeper comprehension of their molecular physiochemical characteristics.

The following section discussing certain widely used methods for producing metal nanoclusters

2.2.5 Monolayer-Protected Method

The monolayer-protected method is a simpler, direct and universal method to produce uniform sized metal nanoclusters. This method is first introduced by Burst *et al* in 1994 for the synthesis of metal nanoparticles protected by monolayer mercaptan ligands [59]. The method uses two-phase method to extract Au(III) chloride, controlled the molar ratio of thiol molecules to Au(III) chloride, and directly synthesized monolayer protected gold nanoclusters. Followed by this invention, the Brust-Schiffin method has been widely used for the synthesis of various nanoclusters stabilized by thiol. This method also named as 'direct-synthesis method'. Tsukuda *et al*. used this method to synthesize and separate a series of SG stabilized AuNCs ($Au_{10}(SG)_{10}$, $Au_{15}(SG)_{13}$, $Au_{18}(SG)_{14}$, $Au_{22}(SG)_{16}$, $Au_{22}(SG)_{17}$, $Au_{25}(SG)_{18}$, $Au_{29}(SG)_{20}$, $Au_{33}(SG)_{22}$, and $Au_{39}(SG)_{2}$., by adopting Busrt-schiffin method [60]. One of the drawback of this method is the low product yield [61].

2.2.6 Etching Method

The etching method is one of the major top-down method for the synthesis of precise MNCs. By the utilization of suitable etching agent, larger metal particles can be etched into NCs of precise size. The etching method is classified into ligand etching and solvent based on selection of etching agent [45]. Edinger *et al*. first time reported the etching property of mercaptan. He found that mercaptan have the ability to remove the Au atoms from the surface of gold nanoparticles and further etched to form AuNCs [62]. Followed by his invention, the etching strategy is widely exploited for the synthesis of various NCs. Pradeep *et al*. synthesized used Au_{25} and Au_{8} from mercaptosuccinic acid protected larger sized gold nanoclusters using SG as the etching agent [63]. Xie *et al*. developed solvent etching method for the synthesis of MNCs. In this method, they altered the hydrophilic and hydrophobic properties of the clusters by electrostatic adsorption, then transferred the clusters from the aqueous phase to the organic phase, etched them under mild reaction to obtain MNCs with uniform size distribution [64].

2.2.7 Template Method

The template method is considered as one of the most popular bottom-up synthetic strategy of MNCs in recent times. In this method uses ligands as reducing and stabilizing agent for the preparation of NCs. The template used to produce NCs are peptides, protein, polymer, dendrimer, DNA, enzyme etc. The protocol for the synthesis of different ligand stabilized nanoclusters, their properties and applications are discussed in the text book entitled "Luminescent Metal Nanoclusters-Synthesis Characterization and applications" [65]. Depending upon the ligands used for stabilization, the properties, structure of the nanocluster varied. The aromatic amino acid present in the macromolecule act as reducing agent and cysteine, amino group will stabilize the nanocluster. The following section will discuss the trends in ligands used for the synthesis of nanoclusters

2.2.8 Trends in ligands used for Nanocluster stabilization

Nanocluster chemistry starts from gas phase clusters. The gas phase cluster is the first reported nanocluster, where the MNCs are formed by evaporation, and it is unprotected. These unprotected clusters are observed to be very reactive to form larger-sized particles [66]. Therefore, proper stabilization techniques should be used for MNC synthesis. The selection of ligands is an important step in the controlled synthesis of the MNCs. The first ligand chosen for the synthesis of MNCs was phosphine due to its high affinity towards metal ions. Briant *et al.* developed a synthetic strategy for the preparation of icosahedral $[Au_{13}\text{-}(PMe_2Ph)_{10}Cl_2](PF_6)_3$ [67]. Followed by a phosphine stabilized cluster, various thiol-stabilized NCs were reported due to the relatively high affinity of sulfur towards metal ions. Due to the insolubility of organic thiol-stabilized NCs in water, water-soluble thiols were introduced to synthesize the NCs. Thiol-stabilized clusters were first introduced by

Whetten *et al* [68]. The ligand used for the stabilization are SG, thiol molecules such as phenylethanethiol, hexanethiol, octanethiol and dodecanethiol- mercaptosuccinic acid (MSA), etc were used for the stabilization of nanocluster by taking the advantages of thiol-gold chemistry [69]. Later new possibilities were raised to create quantum clusters using a macromolecule template. In this green synthesised macromolecules, such as various DNA, protein, polymers and dendrimers, have been used for cluster stabilization and protection [65,70]. The template or ligand used for the stabilization must have a high binding affinity towards the metals (Au, Ag, Pt etc.) in order to prepare highly stable AuNCs with high monodispersed [71]. Figure 2 depicts the core-shell nature of MNCs and can be prepared by selecting appropriate capping ligands [72]. The nanoclusters can be synthesised using different ways such as chemical reduction, photoreduction, hydrothermal, biomineralization and etching, etc. [73].

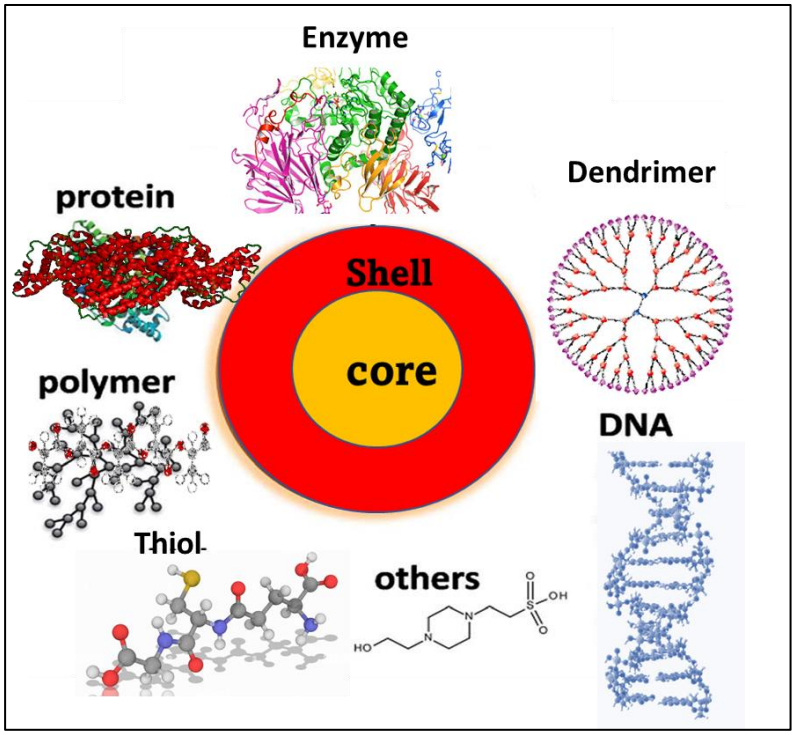

Figure 2. shows a schematic representation of the ligands used for the MNCs synthesis. (core : metal; shell: ligand)

Xie *et al*. first-time developed a biomineralization strategy for synthesizing highly luminescent gold nanoclusters using BSA as protecting and reducing agent [74]. The red luminescent AuNCs comprise 25 gold atoms (Au_{25}). The same strategy is used for the synthesis of various other protein protected metal NCs [47,75]. Recently, Mathew *et al*. synthesized a highly stable fluorescent gluten-stabilized nanocluster. Gluten is a high molecular weight protein derived from wheat; it exhibit enhanced stability towards reactive oxygen species [48].

Reaction duration, pH, temperature, type of ligand, template structure, reducing agent concentration, and Au^{3+}/ligand ratio are crucial synthetic parameters for influencing the structure, size, surface characteristics, oxidation state, and, consequently the optical properties of MNCs [48].

2.3 Key physicochemical properties of MNCs in photocatalysis

MNCs with specific structural designs and resultant exceptional physicochemical, electronic, and optical properties gave birth to a plethora of distinctive materials capable of driving photochemical reactions. Especially, tailoring their optical and electronic parameters could effectively alter their light-harvesting abilities and render us a method to manipulate certain photocatalytic processes by

inducing electron-hole pairs generation to attain maximum quantum yield. For photocatalysis, the major criterion for choosing materials is the strong absorption of solar light [76]. It is worth noting that the sunlight that reaches the earth consists of 3% UV light (280–400 nm), 45% visible light (400–800 nm), and 52% NIR (and IR) light (800–2500 nm). Therefore, to make full use of solar energy, it is very important to improve the light-harvesting capability of semiconductors in visible and NIR regions. This can be realized by designing efficient Au-modified photocatalysts. Both metal nanoparticles and MNCs serve as photocatalysts for solar energy harvesting applications.

On this basis, the deposition of Au nanomaterials on the surface of semiconductors provides an effective way to enhance their light-harvesting capability, especially materials with a large optical gap and, therefore cannot absorb visible light. Due to the strong localized surface plasmon resonance of AuNPs, the AuNPs-modified photocatalysts can exhibit remarkable light absorption enhancement in the visible light region. Similar to AuNPs, few-atom MNCs feature a suitable highest occupied molecular orbital (HOMO)–lowest unoccupied molecular orbital (LUMO) gap for visible and even near-IR light absorption and a long lifetime of excited states for efficient charge separation, make them emerging candidates for solar energy harvesting applications. Both the types MNCs, size, and ligands are fundamental determining factors for the responses to the wavelength of the absorbed light, adding versatility to photo absorption properties as compared to plasmonic particles.

Figure 3 shows the absorption spectrum and solar cells excited with AM 1.5 (100 mW cm^{-2}) of $Au_{25}GSH_{18}$ (where GSH is reduced glutathione). The overlapping region between these two curves is a key component of photocatalysis. For AuNCs, efficient light energy conversion necessitates a slow rate of excited state relaxation. Indeed, $Au_{18}GSH_{14}$ exhibited the highest electron transfer rate and longest excited state lifetime of the NC series [76].

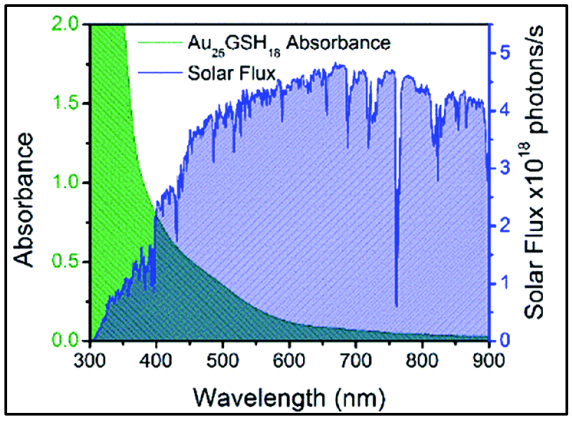

Figure 3. UV-Vis absorption spectrum of $Au_{25}GSH_{18}$, and solar flux for AM 1.5. (Xenon lamp was employed as the solar radiation source). Reprinted with permission from [76]. Copyright 2012 Royal Society of Chemistry

2.4. Optical Properties

2.4.1 Optical Absorption

Metal nanoparticles, having a size range of ~3 nm to 100 nm, obey the plasmonic regime where a single surface plasmon resonance band dominates the optical spectrum and which has a far higher number of atoms than the number of surface molecules that stabilize it (see Figure 4). In such a regime (plasmonic regime), nanoparticles interact with the incident light, and surface plasmon resonance occurs, causing conduction band electrons to collectively oscillate and form characteristic peaks (gold nanoparticle shows surface plasmon resonance at 520 nm) [77,78]. On the contrary, the NCs have a very small number of metal atoms (such as 2, 8, 18, 25, 55, etc.), resulting in an optical spectrum with several bands, distinctive energy levels, and quantum behavior [79].

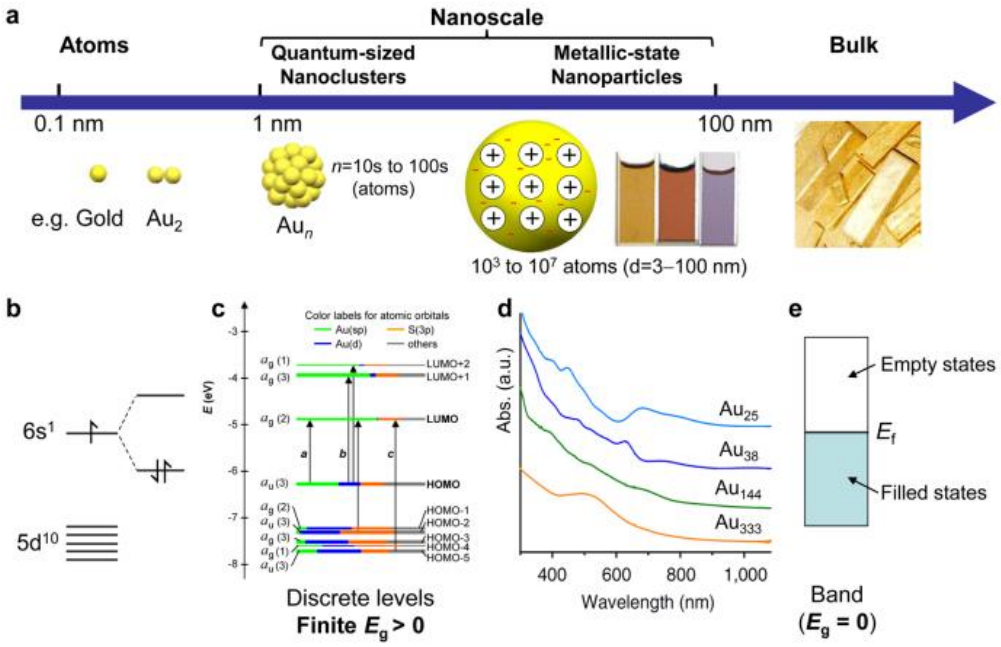

Figure 4. Elucidates the significant distinction between the atomic and bulk regimes concerning size and optical properties. Reprinted with permission from [80] Copyright 2021 Nature.

Figure 4 depicts the electrical transitions between discrete energy levels in MNCs [81,82]. As the particle diameter decreases, SPR peaks disappear gradually, as shown in Figure 4. The Kohn-Sham orbital energy diagram of $Au_{25}SR_{18}$ nanoclusters indicates HOMO composed of triply degenerated 5d10 atomic orbitals and doubly degenerated LUMO, which are 6sp atomic orbitals of gold [83] (Figure 4). Peak 'a' formed due to the HOMO (sp) to LUMO (sp), and peak 'b' is a mixed type band (sp to sp and d to sp) transition. The peak 'c' is formed due to the (d to sp) inter-band transition (Figure 4). Moreover, the absorption of the nanoparticle depends on the metal nanoparticle size. There are several factors that depend on the photocatalytic activity of the catalyst, such as increased visible light absorption, smaller size, higher surface area, optimum band gap, etc. It is reported that photocatalytic activity of the nanoparticle as well as NCs increases with decreasing size of the particle, even though they are absorbed in the visible region or UV region.

Recently, Rongchao *et al*. have carried out a systematic analysis of the size effect on NCs and nanoparticles for photocatalysis. Generally, the smaller NCs have larger specific surface areas and thus more catalytic active sites than the larger NCs. The same observation is noticed in the case of larger metal nanoparticles also [84,85].

2.4.2 Photoluminescence

The photoluminescence property of MNCs opens up possibilities and applications in a variety of fields, including sensing, imaging, etc. [48,86]. The luminescence in MNCs depends on the geometric and electrical structures of the metal core, as well as the ligand shell, alteration in the metal core or ligands, one can tune its optical property. Such NCs can be thought of as a "multi-shell system," comprising a metallic core containing a metal-metal bond, a metal-ligand staple motif as an interface, and surface ligand molecules (see Figure 5). As observed in metal complexes, metal nanocluster also exhibits a similar charge transfer or electron transfer process. These three shells can interact with each other via ligand-to-metal core or ligand-to-metal-metal charge transfer or by directly donating delocalized electrons from the ligands' electron-rich groups [11]. Certain broad tendencies in de-excitation routes have been discovered following visible or near-UV absorption. The experimental and theoretical data from the literature were used to produce the energy diagram in Figure 5. As described in Figure 5, ligand-stabilized atomically precise AuNCs can be viewed as a multi-shell system composed of a gold core (leading to core states), a gold-ligand interface (mainly Au-S bonding leading to "surface" states) and a ligand shell. The three shells may communicate, leading to subtle charge transfer processes. Transitions from molecular orbitals with strong ligand contributions to orbitals with high metal character (LMCT) and from metal-to-metal

electronic transitions can cause near-ultraviolet and visible absorption. Clusters with a core of metal atoms have an initial decay pathway that could result in emission in the visible spectrum. All clusters have a charge-transfer component with a long-lived decay [87]. Furthermore, intersystem crossings are associated with multiple energy transfers (reinforced intersystem crossing (ISC)), which may result in an overall increase in photoluminescence (PL) emission and longer PL lifetimes [79]. The luminescence property is affected by temperature, in such a way that, on decreasing temperature, the HOMO-LUMO gap increases [46].

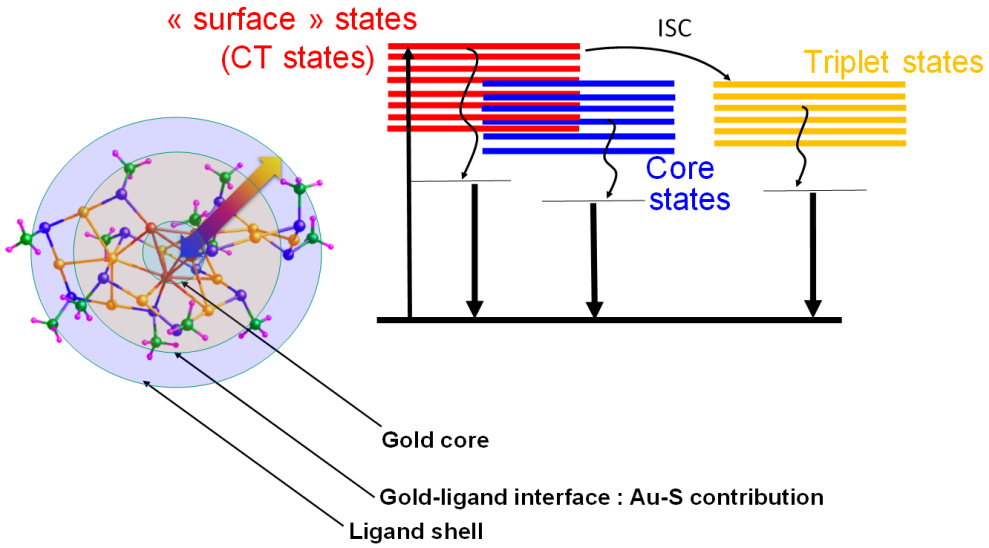

.

Figure 5. Schematic representation of the relaxation pathways of ligand-stabilized atomically precise AuNCs. Illustration of structural bonds and the metal-ligand interface by bringing in AuNCs as an example

2.4.3 Two-photon Absorption:

Two-photon-absorbing (TPA) photocatalyst uses near-infrared low-energy photons [88] for photocatalysis. The unique nonlinear optical (NLO) properties of sub-nanometer core-sized clusters of MNCs exhibit outstanding characteristics [21]. Compared to conventional organic dyes, MNCs show superior two-photon absorption cross-sections (TPA). Although these two-photon processes in small numbered MNCs are well established, the basic photophysical mechanisms behind them still need to be better understood. Generalizations based on complementary theoretical and experimental studies have been made possible by their two-photon absorption properties [89]. It is reported, that the TPA characteristic of AuNCs and AgNCs can be enhanced by the concept of "ligand-core NLO-phone" [90,91]. The different electron or charge transfer processes between the metallic core and ligand are essential for boosting the transition dipole moments leading to enhanced TPA cross sections (as exemplified in Figure 6 with $Ag_{15}(SH)_{11}$ nanoclusters).

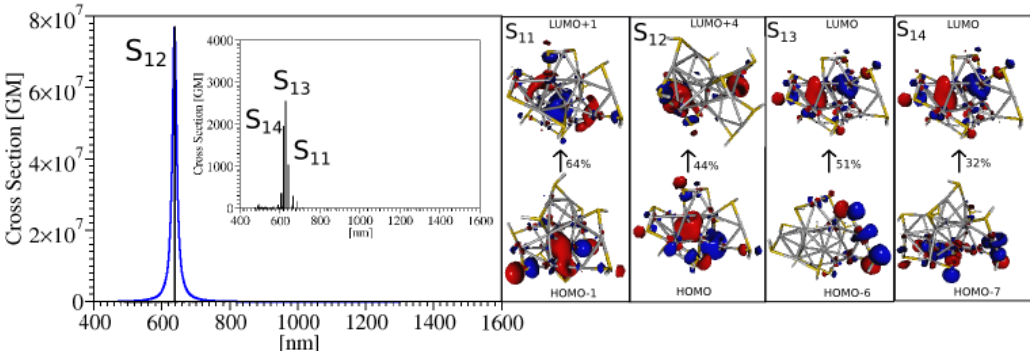

Figure 6. TDDFT TPA spectra of $Ag_{15}(SH)_{11}$ nanoclusters for the lowest energy structure (left panel). Leading excitations responsible for the large TPA cross-sections illustrating the participation of the ligands and the core are also shown (right panel).

2.4.4 Chirality

The photocatalytic activity induced by chiral metallic particles varies with the helicity of the illumination light [92]. MNCs such as gold quantum clusters display fascinating chiral properties [93]. Moreover, the chirality depends mainly on three factors [46]; (a) fundamental chirality is induced first by atomic packing mode, (b) the geometrical isomerisms of the surrounding motifs, and (c) the natural chiral characteristics of the protective ligands and their arrangements covering the metal core [51]. Figure 7a illustrates the two enantiomers of $Au_{28}(TBBT)_{20}$, where the origin of chirality is primarily rooted in the rotating arrangement of the four dimeric staples as well as the arrangement of the bridging thiolates (quasi-D2 symmetry) [40]. Of note, the SR-Au-SR units of AuNCs display chirality, a chiral center at each sulfur atom, and can exist in either a (R, R)/(S, S) trans-configuration or an (R, S) cis-configuration. Indeed, the electronic structure of the sulfur atom in the SR-Au-SR units can be regarded as the sp3 type, where the electrons participate in four tetrahedral kinds of interactions [94]. This bonding motif then creates a chiral center at the sulfur (Fig. 7b).

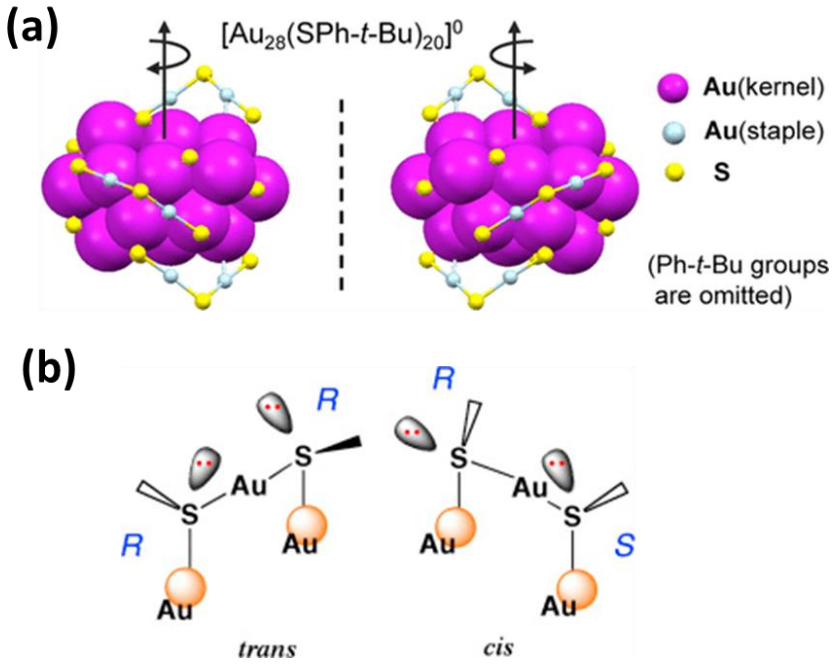

Figure 7. a) The two enantiomers of $Au_{28}(TBBT)_2^0$, where TBBT = 4-tert-butylbenzenethiolate, exhibiting a rod-like Au_{20} kernel consisting of two interpenetrating cuboctahedra. b) Structures of the

(R, R)-trans (left) and (R, S)-cis (right) configurations of two thiolate ligands. Reprinted with permission from [40,94]. Copyright 2016 Elsevier.

2.5. Stability

Metal clusters shielded by thiolates or polymers are attractive possibilities for nanoscale devices [95]. For instance, among various GSH-protected AuNCs, $Au_{25}SR_{18}$ is the most stable one [96]. The isolated Au_{55} clusters exhibit an amazing resistance to oxidation, even when exposed to oxygen atoms and radicals produced by oxygen plasma [97]. When the particle size is decreased to 1.6 nm, the metallic component's spectral weight increases rapidly, indicating that these particles are more oxidation-resistant. This resistance is much more for the case of naked Au_{55} clusters. In addition, ligands influence the stability of MNCs such that the thermal stability of captopril-protected Au_{25} is more when compared to GSH-protected AuNCs [98].

Doping the central metallic core Au_{25} with other elements like Cu and Pd altered the geometric structure and increased the resistance to deterioration, respectively [99]. To illustrate this, Negishi, Y., Kurashige, and co-workers [100] doped the $Au_{25}(SG)_{18}$ with Pd leading to the formation of $Pd_1Au_{24}(SC_{12}H_{25})_{18}$. [$Pd_1@Au_{24}(SC_{12}H_{25})_{18}$] is a binary Pd Au core-shell nanocluster in which Pd is positioned at the center of the icosahedral core of the nanocluster. This has been prepared by replacing the central Au atom of [$Au_{24}(SC_{12}H_{25})_{18}$] with Pd, and the resulting binary mixture exhibit increased thermodynamic stability. The stability against degradation is analyzed by monitoring the absorption spectra of a toluene solution containing [$Au_{24}(SC_{12}H_{25})_{18}$] and [$Pd_1@Au_{24}(SC_{12}H_{25})_{18}$]. They found that [$Au_{24}(SC_{12}H_{25})_{18}$] was stable for up to 30 days in an organic reactor containing toluene as solvent. Thus, they noticed that Pd-doped AuNCs exhibited increased thermodynamic stability and stability against degradation. Similar trends are observed with Pt doped metal nanoclusters [101].

The spectral profile evolves with time, and after 30 days, it resembles that of $Pd_1Au_{24}(SC_{12}H_{25})_{18}$ rather closely and the ESI MS spectrum shows just a single peak that may be ascribed to $Pd_1Au_{24}(SC_{12}H_{25})_{18}$ [102]. The strong interaction energy between Pd and $Au_{24}(SC_{12}H_{25})_{18}$ was proved by the DFT calculation of Jiang *et al*. Consequently, with the $Au_{24}(SC_{12}H_{25})_{18}$ frame, Pd develops an intermetallic structure and on the strength of this $Pd_1Au_{24}(SC_{12}H_{25})_{18}$ presents higher thermodynamic stability than $Au_{25}(SC_{12}H_{25})_{18}$. On the other hand, doping the $Au_{25}(SC_2H_4Ph)_{18}$ with Copper reduced its overall nanocluster stability [103]. Doping with copper formed $Cu_{-1}Au_{-24}(SC_2H_4Ph)_{18}$. In comparison to $Au_{25}(SC_2H_4Ph)_{18}$, the optical absorption spectra moved toward lower energy, suggesting that the HOMO-LUMO gap has shrunk.

The electronic density of states study of $Au_{25}(SR)_{18}^{1-}$ reveals its electronic state of Au_{13} core (8 electrons) protected by six [$(SR)_3Au_2$] complexes [68]. The superior stability for $Au_{25}(RS)_{18}$ is achieved by structural toughness and an 8 e- shell of delocalized Au(6s) electrons for the anion. The gold nanocluster superatom model expands the jellium model [104] to explain multiple ligand-protected AuNCs with closed valence-electron shells (2, 8, 18, 20, 34, 40, etc.). The metal core is regarded as a single atom in the super atom hypothesis. The extraordinary stability of these NCs emerges from the regular closure of outer electronic shells [105]. Even if strong structural and electronic stabilization occurs for $Au_{25}(RS)_{18}$, the nature of protecting ligands affect the stability of the cluster. The role of isomer was studied using para, meta, and ortho MBA stabilized NCs [106]. Figure 8 shows the isomeric effect of MBA on the stability of $Au_{25}(MBA)_{18}$NCs. The steric hindrance of the carboxylic groups plays a major role. The m-MBA and o-MBA ligands stabilized nanocluster shows noticeable steric hindrance at the gold core's surface, which leads to significantly lowering the binding energy required for the fragmentation of Au-S bond

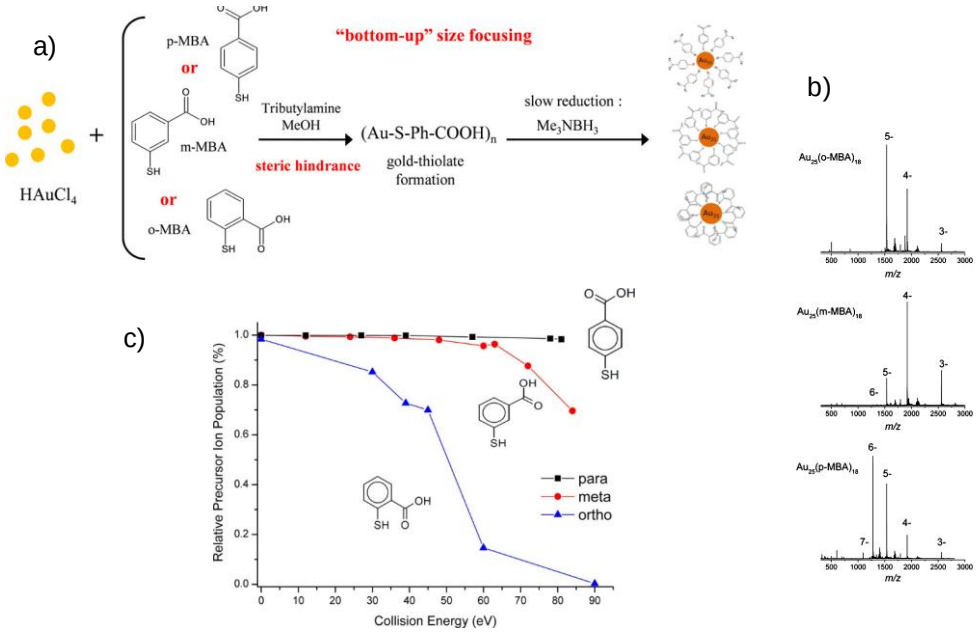

Figure 8. a) diagram shows the synthesis protocol of different structural MBA isomers stabilized $Au_{25}(MBA)_{18}$ NCs. b) ESI mass spectra Au_{25} clusters c) collision-induced dissociation breakdown curves for the 4– charge state of o/m/p-MBA stabilized. Reprinted with permission from [106] Copyright 2018 American Chemical Society.

3. Application of Nanoclusters in Photocatalysis

Over time, research on the relevance of cleaner fuels, alternate potential energy sources as well as tools to alleviate, pollution have been gainful. Research on visible light photocatalysis over the past decade has drawn much attention in this line. Semiconductor heterogeneous nanotechnology-based photocatalysts lasted long enough and showcased their prominence in this specialty. At present, material chemists are busy preparing competent monometallic or hybrid entities by combining conventional semiconductors with suitable pre-catalyst/co-catalysts to bring about the best results in photocatalysis. MNCs have proved their supremacy in multiple economic and sustainable processes of photocatalysis such as photodegradation of organic pollutants, photocatalytic H_2 splitting, photoreduction of CO_2, oxidation and hydrogenation reactions, etc. The fast recombination of e^-/h^+ of semiconductors, noble metal/metallic/non-metallic moieties on semiconductors support extending photocatalytic activity towards the visible range.

Photostability and recyclability are considered major factors to consider during photocatalysis. The photocatalytic stability of NCs has been improved by incorporating a suitable catalyst, which further enhances the efficiency of the catalysis [107,108]. Duan and his co-workers developed TiO_2 supported AgNCs for the photocatalytic removal of NO. They have studied the photostability of the TiO_2-NCs shows excellent photostability and recyclability [109]. A similar observation has been observed by Yu *et al*. and they found that TiO_2 nanocrystals supported-$Au_{25}(SR)_{18}$ show outstanding photostability in cycle studies and enhanced photoactivity for the methyl orange (MO) degradation [110].

The following section discusses the role of MNCs in photocatalytic as cocatalysts as well as catalysts in various light conversion processes.

3.1 Photodegradation of organic pollutants

Globalization-led industrialization, to satisfy the needs of the world's population, has led to a steep rise in harmful pollutants in the environment at an alarming rate. The organic pollutants from textile industries majorly constitute azo dyes, while inorganic pollutants hold oxidized heavy metals. These under-treated materials containing carcinogenic effluents are being dumped into the soil and water and have already created damages beyond repair to humans as well as to the aquatic flora

and fauna. Initiating action plans to safely remove them without the formation of other stable secondary pollutants demanded scrutiny. Methyl orange (MO), rhodamine B (RB), malachite green (MG), and methylene blue (MB) are some of the commonly found, dyes that have been present in industrial effluents. Reactive oxygen species (ROS) such as superoxide radicals ($O^{2-\cdot}$) and hydroxyl radicals ($OH^{-\cdot}$) are the prime contributors and starting materials in the degradation of these toxic materials [111].

Titania (TiO_2), ZnO, SiO_2, Nb_2O_5, etc. have been reported widely as a solution for pollution initiated by organic pollutants through photodegradation [112,113]. These semiconductor systems ensure photostability, low cost, mere toxicity, and a fundamental level of oxidative ability. However, the fast recombination of electron-hole pairs before taking part in the surface reactions reduces the rate of the photoreactions. Grafting small nanoparticles on TiO_2, which can act as a co-catalyst to efficiently absorb in the visible and possibly NIR range, acts as an electron acceptor, and in turn, suppresses the recombination of photo-excited electron−hole pairs would dramatically enhance their efficiency. As the research studies progressed, metal nanoparticle-incorporated versions of semiconductors became the focal point. MNCs linked to semiconductor systems as support have profoundly influenced the works in photocatalytic degradation of cationic and anionic dye pollutants as they could enable us to engineer the bandgap width [114,115].

Zhu and co-workers prepared AuNCs coupled with toroid structured per-6-thio-β-cyclodextrins placed on the TiO_2 surface (TiO_2-Au NCs@β-CD) provided a better space for the Au cores to interact with the incoming pollutants through a host-guest interaction trap [116]. This synergistic effect between the nanocluster metallic core, peculiar ligand cavities, and support system increased the photodegradation rate of methyl orange (MO) to 98% in 10 minutes. Concurrently, the integrated material's rate constant values for photodegradation (1st cycle=0.31min^{-1}, 5th cycle= 0.15min^{-1}) were phenomenal in comparison with TiO_2(1st cycle= 0.12min^{-1}) even after five cycles. Sharma and co-worker studied Au-TiO_2 conjugated nano-assembly as photocatalysts under both UV and visible light by utilizing methylene blue and a common organic pollutant carbendazim [117].

The mechanism for photocatalytic degradation of dyes using Au-TiO_2 can be explained by following reaction pathways

$$Au + h\nu \rightarrow Au\bullet$$

$$Au\bullet + TiO_2 \rightarrow h+(Au) + e-(TiO_2)$$

$$e-(TiO_2) + O_2 \rightarrow TiO_2 + \bullet O^{2-}$$

$$\bullet O_2- + H^+ \rightarrow HOO\bullet$$

$$HOO\bullet + e-(TiO_2) + H^+ \rightarrow H_2O_2 + TiO_2$$

$$H_2O_2 + e-(TiO_2) \rightarrow \bullet OH + OH^- + TiO_2$$

$$h+(Au) + H_2O \rightarrow Au + H^+ + \bullet OH$$

$$h+(Au) + OH^- \rightarrow Au + \bullet\ OH^-$$

$$\text{Organic pollutants} + O_2-\bullet \text{ or } \bullet OH^- \rightarrow CO_2 + H_2O + \ldots.$$

Gowswami *et al*. created colloidal nanocomposite material with TiO_2/Nb_2O_5 conjugated to silver NCs with captopril as a ligand. They have varied the niobium loading in the incorporated product to investigate the adhesion of the material towards cationic and anionic dyes as well as their photodegradation capability [118]. As per the analysis, the mentioned nanocomposite with 48.1% niobium loading and Ag NCs resulted in the ternary junction, which narrowed down the recombination rates and the surface acidity caused the Ag NCs ligands' end groups to polarize COO^-, thereby attracting the cationic dyes for effective 100% degradation with high photostability. Spectroscopic techniques validate that Ag NCs are the reason behind absorption in the visible light region and act as oxidative sites. They also initiate electron transfer from the valence band of the NCs

to the conduction band of nanocomposites. Samai's group made polyethylene imine template Ag NCs incorporated with CeO_2 nanoparticles for degrading acridin red dye photo-catalytically [119]. XPS mechanistic work and radical experiments pin down their radical pathway leading to 42% to 80% degradation in 2 hours with 1.07% and 3.10% Ag NCs loading, respectively. The reduction potential and two oxidation potentials vs NHE values were recorded with cyclic voltammogram to be -0.64V, 0.07V, and 1.03V, respectively (Figure 9).

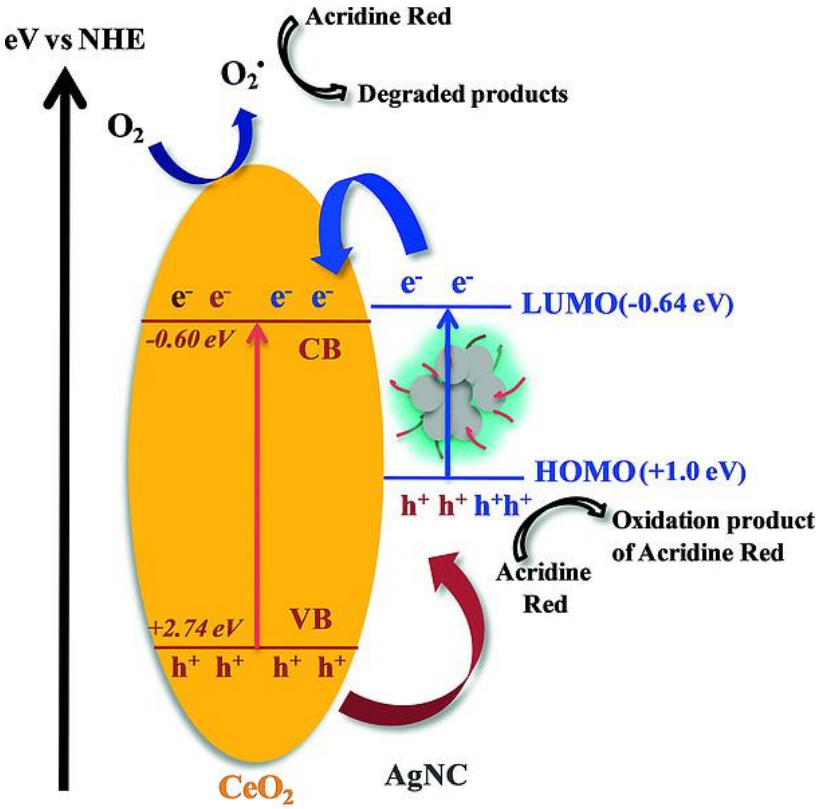

Figure 9. Schematic representation of the mechanism of the photocatalytic degradation of Acridine Red in the presence of the AgNC/CeO_2 nanocomposite under UV light irradiation. Reprinted with permission from [119] Copyright © 2018 John Wiley & Sons.

ZnO nanoparticles decorated with Ag NCs were established as a prospective candidate for Orange II (OII) dye degradation under both UV and white light by Rodriguez and co-worker [120]. Atomic force microscopy (AFM) confirmed the deposition of NCs moiety on ZnO rather than the substitution of the metallic core itself. Additionally, the optimal loading range of Ag on ZnO was found to be 1.3% w/w and it indeed ensures an ample number of interaction sites for the pollutants to approach ZnO nanoparticles. Figure 10 shows the spectroscopic and morphological characterization of AgNC-decorated ZnO nanoparticles. Vidal *et al*. formulated green emitting stable closed-shell electronic structured and recyclable CuNCs to degrade MB under UV and Visible light irradiation [121]. UV-Vis data and administered multiple photoluminescence emission peaks were an indication of a mixture of clusters and LDI-TOF spectrometry approves proposed structural formulas of Cu NCs: $[Cu_{18}(CH_3COO)(OH)]^{-2}$ and $[Cu_{34}O_2(CH_3COO)_3N(C_4H_9)_3Na]^{-2.}$

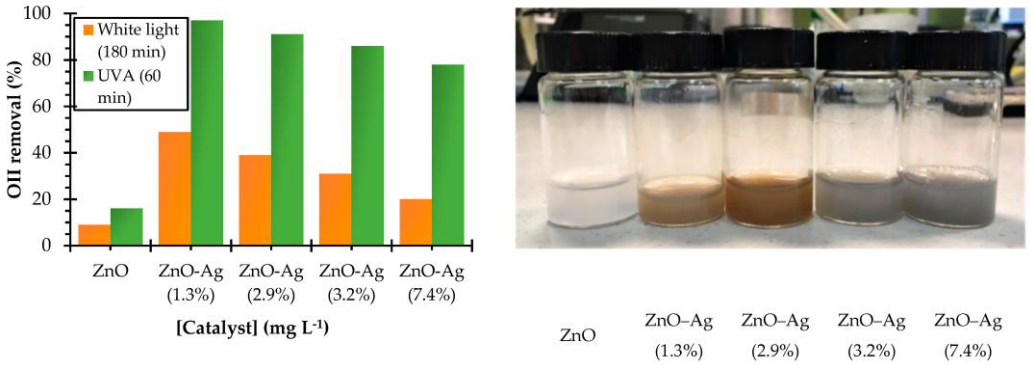

Figure 10. Silver loading effect on photocatalytic performance. The values in brackets correspond to the percentage of Ag in each NC (left); Aqueous suspensions of ZnO-NPs and ZnO–Ag NCs with different silver loadings (right). Reprinted with permission from [120] Copyright 2019 MDPI.

Light-steered preparation of 3-mercaptopropyl trimethoxy silane (MPTS) stabilized AuNCs, and their performance in photodegradation of MB was examined by Zhou *et al*. [49]. It was observed that the NCs decolourize the dye progressively, and the colour fades completely in 60 mins.

Man Cao and his co-worker synthesized a self-assembled silver nanocluster for photocatalytic degradation of sulfur mustard simulant (2-chloroethyl ethyl sulfide, CEES), a toxic vesicant against human proteins and DNA, which can cause skin blisters, eye, and respiratory system irritation, and even fatal damage. The silver cluster assembled material is prepared using a photosensitizer 5,10,15,20-tetra(4-pyridyl)porphyrin (TPyP) as the organic linker and which linked with 12-core silver chalcogenolate cluster to form $[Ag_{12}(St\ Bu)_6(CF_3COO)_3(TPyP)]_n$, (designated as Ag_{12}TPyP). They reported 98 % degradation of CEES with 1% loading [122,123].

Wen and co-workers developed a highly stable core-shell type catalyst for photo-redox reactions. The photostability of the nanocluster was improved by loading it on a SiO_2 sphere by utilizing multifunctional branched poly-ethylenimine (BPEI) as a surface charge modifying, reducing, and stabilizing agent. Then TiO_2 was coted SiO_2-Au GSH clusters-BPEI to form SiO_2-Au GSH clusters-BPEI@TiO_2 core-shell structure further significantly improve the photocatalytic efficiency for dye degradation of organic dye (Rh B) [124].

3.2 Oxidation and hydrogenation processes

Application of NCs in oxidation and reduction processes is still underway. Oxidation and hydrogenation reactions in most reported cases specifically depend on their electronic structures, as electron-hole separation remains the key to it. Researchers have carried out typical oxidation-reduction reactions like high selectivity styrene oxidation [125], aerobic oxidation of amines to imines [126], and cyclohexane or phenol derivatives [127] in the presence of MNCs, especially AuNCs. In 1987, Haruta and co-workers were the first to initiate oxidation of CO with few atom AuNCs along with α-Fe_2O_3, NiO, and Co_3O_4 at low temperatures [128]. After two decades, a mechanistic view of photocatalysis of Au_{25} nanoclusters with TiO_2 as support under visible and near-infrared emissions was illustrated by Kogo and co-workers [129]. They attached AuNCs to TiO_2 so that the excited electrons could be transferred to the conduction band of TiO_2 with ease and can aid in the reduction of Ag+ in the counter electrode, and the generated holes (h^+) could perform oxidation of donors (phenol derivatives or formic acid) in working electrode (Figure 11).

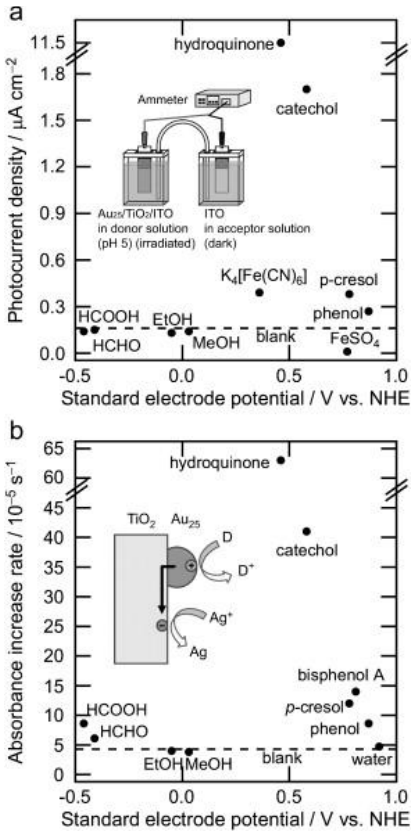

Figure 11. Photocatalytic oxidation ability. Reprinted with permission from [129] Copyright 2010 Elsevier.

Similarly, Zhu *et al*. did a comparative study to figure out the capabilities of a set of superatoms to oxidize styrene- $Au_{25}(SR)_{18}$, $Au_{38}(SR)_{24}$, and $Au_{144}(SR)_{60}$ with diameters of 1nm, 1.3nm, and 1.6nm respectively [130]. However, their studies reassured the size and electronic structure dependence of photocatalytic abilities, and Au_{25} NCs gave the highest average of ~27 ± 1.0% as the smaller the superatom, the higher the HOMO-LUMO gap (1.3eV). Later, Chen & group loaded $[Au_{25}(PPh_3)_{10}(SR)_5Cl_2]$ on P_{25} to convert benzylamines to imines; TOF was recorded to be 1522 h^{-1} for 4-methylbenzene and other amines too showed appreciable conversions (73-99%) [126]. The attempts to learn the possible conversion route using time-dependent density functional theory (TD-DFT) calculations, Fourier-transform ion cyclotron resonance mass spectrometry (FT-IC-MS) with electrospray ionization (ESI), and trapping intermediates with scavengers ($K_2S_2O_8$ and ammonium oxalate) confirmed the presence of +2 charge on the cluster. Hence the photo-catalytically induced electron could lead to oxygen radical formation and thereby persuade conversions. Studies with organic support too have gained momentum over the years. Gold nanocluster with organic supports (polyvinylpyrrolidone (PVP) & polyperoxyacetic acid (PAA)) was analyzed by H.Tsunoyama and co-workers. X-ray photoelectron spectroscopy (XPS) & X-ray absorption near edge structure (XANES) reinforced the existence of negatively charged clusters which led to the production of superoxide- or peroxy-radicals required to jump-start the photocatalytic reactions [131]. Their activities and recyclability were keenly observed for CO oxidation. In addition, this set of reactions enlightened the research community about the prime role of NCs in oxidation and reduction reactions.

Hamoud and co-workers studied the photocatalytic activity of Ag NCs encapsulated into zeolite (ZX-Bi zeolite) for photooxidation of methanol under visible light. They have found that the Ag/ZX-Bi exhibits very low, activity compared to the activated sample at 200 °C (Ag/ZX-Bi_200) [132].

3.3. Photocatalytic H_2 production

3.3.1. Hydrogen Evolution Reaction

The demand for green energy sources better suited for the environment is rising due to the reduction and environmental pollution generated by conventional energy resources. While the distinct qualities shape, hydrogen gas is an acceptable renewable energy source for a sustainable future [133]. Ahluwalia and co-workers studied the fuel economy of hydrogen-fueled fuel cell (H_2-FCV) vehicles and common gasoline-fueled passenger cars in 2003 [134]. In 1972, Fujishima *et al*. first discovered that water could be divided into H_2 and O_2 in the presence of light [1].

Catalysts based on the metals such as Ti, Cobalt, Nickel, Iron, and Molybdenum are widely used as catalysts for electrochemical H_2 production [135]. After that, the catalytic efficiency of metal oxides and metal nitrides was enhanced by incorporating suitable cocatalysts into these semiconducting materials. The Co-catalytic activity of metal nanoclusters has been studied in the recent past due to its excellent optical, electronic, and catalytic activity. The NCs were incorporated into various semiconductors to enhance the catalytic activity by suppressing the electron-hole recombination rate.

Kamat *et al*. studied the photoelectrochemical and photocatalytic production of H_2 using GSH stabilized AuNCs-TiO_2 film hybrid system under visible light irradiation [135]. Liu *et al*. carried out a detailed investigation on the photocatalytic activity of AuNCs as cocatalysts in highly ordered nanoporous layer-covered TiO_2 nanotube arrays (NP-TNTAs). The photocatalytic activity of NP-TNTAs/AuNCs was analyzed by monitoring the photodegradation of organic dyes, photocatalytic reduction of aromatic nitro compounds, and photoelectrochemical water splitting [136]. Similarly, AuNCs loaded on $SrTiO_3$ were studied for HER and found the enhanced catalytic activity of $SrTiO_3$ in the presence AuNCs as Cocatalyst [137].

The quantum confinement of MNCs enables the charge transfer, easy adsorption, and desorption of intermediates and thereby fastens the photocatalytic hydrogen evolution reactions (HER) [29]. Sub-nanosized clusters of silver adsorbed on specific sites of gold nanorods (GNRs) disturb the growth symmetry of Au facets and lead to anisotropy [138]. In the presence of a hole scavenger, namely ethanol, and in the absence of electron scavengers like O_2, the photoelectrons accumulate in GNRs with Ag clusters. Moreover, on low UV light irradiation, Ag_3 clusters at a concentration of 0.43μg within the GNRs show high H_2 production efficiency of 10%. Similarly, the loading of 1 wt% of sub-nm Au clusters in CdS uplifts the photocatalytic H_2 production about 35 times that of the unmodified CdS under visible light [139]. The comparison of sub-nm Au-loaded CdS with Pd/CdS and Rh/CdS of similar size revealed that the 3-nm sized Au/CdS was a better co-catalyst.

Likewise, monolayer niobate (HTi_2NbO_7) nanosheets with Pt NCs proved themselves as potential photocatalysts for high H_2 production [140]. Monolayer niobate nanosheets enable the charge separation between photoelectrons and holes and display 5 times higher photocatalytic H_2 production than that observed in its layered form. 1 wt% Pt NCs loaded to niobate nanosheets via photoreduction presented increased activity due to the close contact between the HTi_2NbO_7 nanosheets and Pt nanocluster. On light irradiation, electrons migrated to the conduction band moved to the surface of nanosheets. Since Pt has a higher work function than niobate nanosheets, these electrons on the surface of nanosheets transfer to Pt and form H_2.

While Cheng and co-workers [138] revealed the effective co-catalytic effect of sub-nano-sized Pt-Au alloy clusters in photocatalytic H_2 evolution. The synergistic effect of 0.5 wt% of both Pt and Au clusters dispersed in TiO_2 (Pt-Au/T) creates increased charge separation, and 80.1 μmol h^{-1} of H_2 is evolved with a quantum efficiency of 50% at 365nm. As with HER, a similar strategy has been established for enhanced efficiency for OER by using the nanocluster as a cocatalyst [141]. Au_{25} NC-$CoSe_2$ composite was studied for OER activity and found enhanced OER activity in the presence of $Au_{25}/CoSe_2$ obtained a current density of 10 mA cm^{-2} at a small overpotential of ~0.43 V (cf. $CoSe_2$: ~0.52 V). The ligand and gold cluster size can also tune the catalytic performance of the composites. Yang *et al*. also illustrated the effect of heteroatom doping on the photocatalytic activity of $PtAg_{24}$-loaded graphitic carbon nitride ($PtAg_{24}/g\text{-}C_3N_4$) and found that $PtAg_{24}/g\text{-}C_3N_4$ shows higher efficiency for photocatalytic H_2 production than $Ag_{25}/g\text{-}C_3N_4$ alone [142].

Similar to Au, Ag, Pt, and Pd NCs, Cu nanocluster is also used as a photocatalyst for various photoreactions. Barbara *et al*. developed in situ formations of CuNCs over hexaniobate nanosheets for photocatalytic H_2 evolution reaction. The electrostatic interactions between Cu and Ni lead to the

decoration of NCs over hexaniobate nanosheets, increasing electron-hole separation and thus enhanced efficiency for H_2 evolution [121,143–145].

3.3.2. Photocatalytic Water Splitting

SG stabilized AuNCs ($Au_{25}(SG)_{18}$) were incorporated on $BaLa_4Ti_4O_{15}$ for photocatalytic water splitting. The catalytic activity of sub-nanometer-sized Au-BaLa4Ti4O15 compared with larger-sized gold nanoparticles found 2.6 times higher catalytic activity for AuNC composite [146]. Recently, Hanieh Mousavi and Co-workers studied the photocatalytic production of H_2 using AuNCs as Co-catalyst. They have prepared a nanocomposite (Au_{101}NC-$AlSrTiO_3$-rGO) containing AuNCs, RGO, and $AlSrTiO_3$, and the composite showed enhanced photocatalytic water splitting under UV light irradiation [147].

Moreover, by monitoring nanocluster size, the photocatalytic activity of the whole system can be varied. Heiz, Feldmann, and co-workers modified cadmium sulfide (CdS) nanorods with a series of Pt NCs such as Pt_8NC, Pt_{22}NC, Pt_{34}NC, Pt_{46}NC, and Pt_{68}NC and found that Pt_{46}/CdS exhibits the highest activity for photocatalytic water splitting, due to the well-known quantum confinement effect, where the bandgap increases with a decrease of the NC size [148]. Rongchao and his co-worker reported a detailed review of the effect of the size of NCs in photocatalysis [85].

The photocatalytic activity of the co-catalyst was studied by monitoring the doping of heteroatom on the NCs. Negishi *et al*. demonstrated that doping Pt on Au_{25} NC enhances the water-splitting activity, while Pd doping reduces the water-splitting activity. They proposed that the doping position plays a role in the catalytic activity. The doped Pd is located at the surface of the metal-cluster cocatalyst, whereas Pt is located at the interface between the metal-cluster cocatalyst and the photocatalyst [149]. In addition to the above studies, scientists are exploring the efficiency of photocatalytic water using composites, including MNCs with g-C_3N_4 nanosheets, TiO_2, etc [150].

3.5 Photocatalytic CO_2 reduction

Nowadays, reducing greenhouse gas emissions from various photovoltaic (PV) systems has become one of the scientific community's primary concerns [151]. Carbon dioxide (CO_2) is one of the chief greenhouse gases that influence the heat content of the earth's atmosphere [1]. With a focus on reducing CO_2 emissions, novel technologies are adopted for the production of commodity chemicals by using CO_2 as feedstock [152]. The conversion of CO_2 to value-added chemicals or other hydrocarbon fuels such as methane, ethylene, and carbon monoxide by utilizing energy from non-fossil resources such as solar energy increases carbon recycling and assists in fuel production [153,154]. Solar-driven transformation of CO_2 into valuable products could be achieved through two major approaches such as photocatalytic and electrochemical CO_2 reduction processes [155]. In 1978, Halmann utilized p-type semiconductors for the photo-electrochemical reduction of CO_2 [156]. Methanol and Carbon monoxide obtained from the conversion of CO_2 are identified as useful feedstocks [157]. The former synthesizes other hydrocarbon fuels, while the latter is used for Fischer–Tropsch syntheses.

CO_2 is a thermodynamically stable molecule, and catalysts assist the electrochemical CO_2 reduction reactions and aid in achieving the desired product [158]. MNCs possess ultrafine structure, electronic and optical properties [34] and function as electrocatalysts and photocatalysts [27]. Various features of MNCs, such as size, core, composition, surface ligands, charge state, and geometry, influence their electro and photocatalytic behaviors [27]. Colombo Jr and co-workers studied femtosecond electron-hole recombination in TiO_2- NCs and explained the intra-cluster dynamics [159]. The study demonstrates the steps involved in electron trapping, recombination, and formation of long-lived species. Kauffman *et al*. studied the weak reversible interaction between CO_2 and $Au_{25}(SC_2H_4Ph)_{18}^-$ clusters [160]. The electrochemical reduction of CO_2 using Au_{25} catalyst in aqueous 0.1 M $KHCO_3$ showed maximum CO production at -1.0 V with 100% Faradaic efficiency. The electrochemical CO_2 reduction performance of silver NCs confined in bovine serum albumin (AgNC@BSA) is enhanced via polyoxometalates $[\alpha\text{-}SiW_{12}O_{40}]^{4-}$ [161].

The presence of suitable photocatalysts possessing features such as high light absorptive power, convenient catalytic sites, and low activation energy enhances the photocatalytic reduction of CO_2

[162]. The small-scale size of MNCs of about 2nm, interfacial surface, energy gap, tunable chemical properties, and quantum confinement are the advantages of ultrafine MNCs for CO_2 reduction over metal nanoparticles [163]. Titanium dioxides or titania are widely used semiconductors and have a broad range of applications, including the photoreduction of CO_2 [164]. Doping and decoration with other elements or metal ions strengthen its photocatalytic activity by reducing its band gap. In addition to these elements, attaching NCs to TiO_2 makes it a potent visible light photocatalyst [165]. Inserting Ti^{3+} ions into the TiO_2 creates isolated states in the presence of UV and visible light. The electrons are trapped in these states, and due to recombination with charge carriers' photocatalytic activity is decreased. On combining Ti^{3+} introduced TiO_2 with NCs of Cu (II) oxides (i.e., Cu (II)-TiO_2@Ti^{3+}), electrons from the isolated states of Ti^{3+} move to the surface of Cu (II) NCs. Hence, the photocatalytic activity of Cu (II)-TiO_2@Ti^{3+} under visible light is raised and decomposed gaseous 2-propanol (IPA) completely to yield ~18 μmol CO_2 generation. On UV irradiation, copper oxide (Cu_xO) NCs incorporated in strontium titanate nanorod thin film [166] and niobate sheets [144] showed selective CO production from photocatalytic CO_2 reduction.

Product selectivity towards CH_4 and CO is shown by brookite TiO_2 quasi nanocubes (BTN) on surface decoration with Cu-NCs (Cu-BTN) under xenon lamp irradiation [167]. XRD diffraction peaks exhibit the presence of Cu-NCs only on the surface of BTN. The total consumed electron number (TCEN) is utilized for examining overall photocatalytic CO_2 reduction. At a 1.5 % optimum concentration of Cu-NCs in BTN, maximum photoactivity with TCEN of 150.9 $\mu molg^{-1}h^{-1}$ and highest production rate of 4.23 $\mu molg^{-1}h^{-1}$ CO and 17.81 $\mu molg^{-1}h^{-1}$ CH_4 is observed (Figure 12).

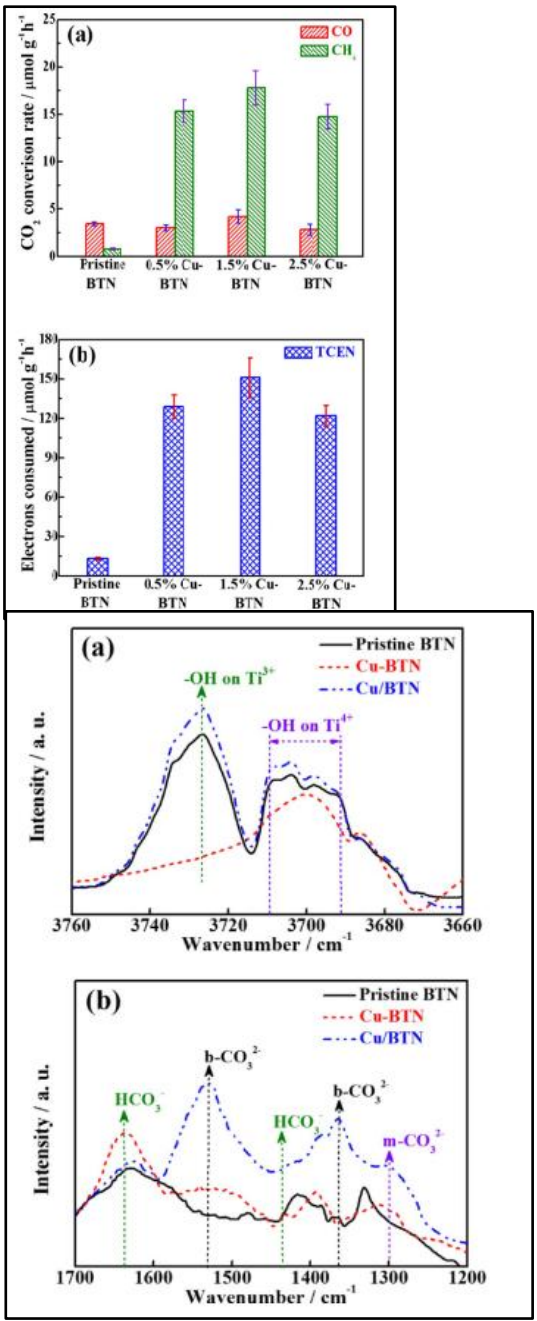

Figure 12. CO/CH_4 production rates (a) and the corresponding total consumed electron numbers (TCEN) (b) for the CO_2 photoreduction over pristine BTN and Cu-BTN production with different Cu loading contents during the initial 2 h of irradiation. Reprinted with permission from [167] Copyright 2017 American Chemical Society.

Figure 13. In situ DRIFTS IR spectra of H_2O (a) or CO_2/H_2O vapor (b) interaction with pristine BTN, 1.5% Cu-BTN, and 0.5% Cu/BTN. Reprinted with permission from [167] Copyright 2017 American Chemical Society.

In situ, DRIFTS IR spectra suggested CO_3^{2-} intermediate for CO formation and HCO_3^- for CH_4 (Figure 13a). Cui *et al*. worked on the role of bridging ligands and metal ions grafted to AuNCs in the photocatalytic conversion of CO_2 to CO [168]. The functionalization of L-cysteine with SG-protected Au nanocluster (Au-GSH NCs) helps bind metal cations such as Fe^{2+} Co^{2+} Ni^{2+}, and Cu^{2+} and thus improves the selective CO production. Under visible light along with CO_2 and H_2O, Co^{2+} cation within Au nanocluster (Auc-C-Co) at an optimum concentration of 4 µmol exhibited maximum CO production of 3.45 µmol. Great-1h-1. Similarly, via 3-mercaptopropionic acid (MPA), Co^{2+} is grafted to the surface of Au nanocluster (Au_c-MPA-Co) and exhibited high-rise in photocatalytic activity compared to (Au_c-C-Co) through strong interlinkage between S-metal cation (Figure 14).

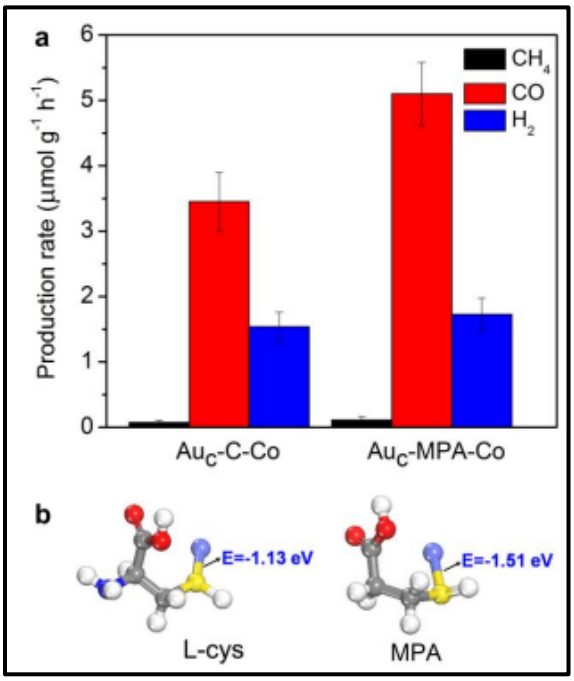

Figure 14. (a) Average production rates of CH_4, CO, and H_2 in light driven CO_2 reduction with H_2O in the presence of TEOA, catalyzed by 10-mg Au_c-MPA-Co grafted with 4 µmol Co^{2+} (b) The

binding energy of S-Co bond in the coordination of Co with L-cys and MPA. Reprinted with permission from [168] Copyright 2018 American Chemical Society.

Zhang and co-workers [144] developed a quasi-ternary complex consisting of polymethacrylic acid stabilized Ag NCs (AgNCs-PMAA), carbon monoxide dehydrogenase (CODH), and TiO_2 nanoparticles and under visible light CO_2 reduction results generation of CO with 20 s^{-1} turnover frequency at 25℃. Jiang, *et al*. [169] upgraded the chemical stability of AuNCs (Au-NCs) by combining with a metal-organic framework (UiO-68) through N-Heterocyclic carbene stabilizing ligands (NHC) and denoted as AuNC@UiO-68-NHC. The photocatalytic activity AuNC@UiO-68-NHC enhanced due to strong covalent bond formation between AuNCs and UiO-68 facilitated by Au-NHC bridges. This enabled easy movement of excited electrons from the Fermi levels of AuNCs to the conduction band of UiO-68-NHC and thus, the recombination of photogenerated electrons and holes is reduced (Figure 15) [169].

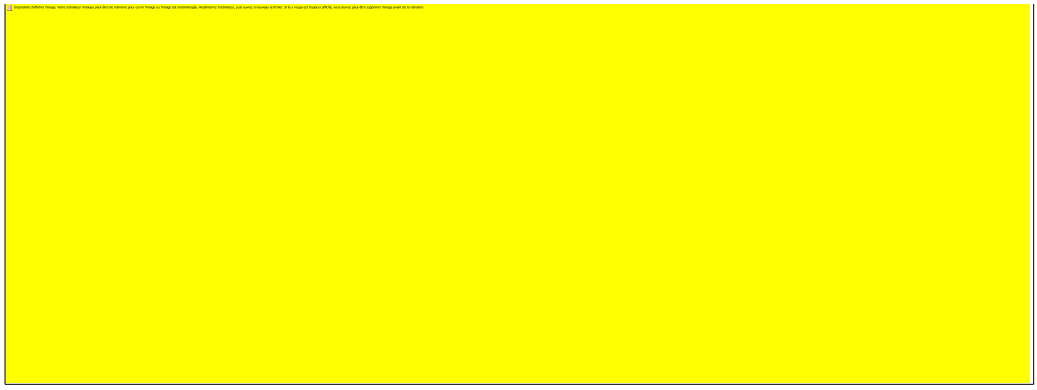

Figure 15. (a) CO evolution period of photocatalytic CO_2 reduction using UiO-68-NHC, Au-NC@UiO-68-NHC, UiO-68-NH_2, and Au/ UiO-68-NH_2 as photocatalysts upon AM 1.5G irradiation. (b) Time courses of photocatalytic CO_2 reduction on Au-NC@ UiO-68-NHC under AM 1.5 G irradiation for 12h, with evacuation every 4 h (dashed line). Reprinted with permission from [169] Copyright 2021 Wiley.

The selective production of CO and the presence of CH_4 and H_2 as side products is observed. Billo and co-workers developed an effective photocatalyst with dual sites by making oxygen vacancies in Ni-NCs loaded in black TiO_2 (Ni/TiO_2[Vo]) [170]. Ni and oxygen defective sites act as dual sites, lessen the C-O bond strength and support the separation of charge carriers (Figure 16). On light irradiation from a halogen lamp, Ni/TiO_2[Vo] produced 10 μmol g-cat^{-1} of acetaldehyde,18 times higher than TiO_2. Thus, the study refers to a different approach for enhancing photocatalytic CO_2 reduction by introducing active dual sites in photocatalysts. Recently, El-Roz *et al*. prepared a silver nanocluster-based catalyst for

onverting formic acid to CO_2 and H_2 under visible light irradiation. Here the nanocluster was incorporated into a nano-sized zeolite crystal [169].

Table 1 summarizes the utilization of nanocluster as a co-catalyst/catalyst for various photoreac-

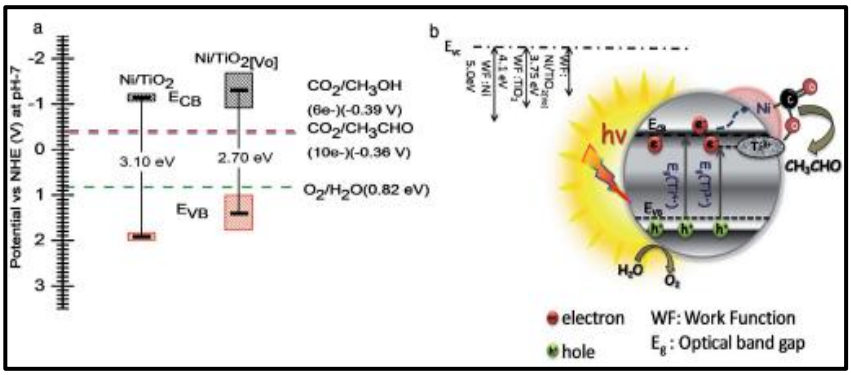

776 tions.

777

778 **Figure 16**. (a) Band edge positions. (b) Schematic illustration of photocatalytic CO_2 reduction
779 mechanism of Ni/ TiO_2[Vo]. Adapted from Ref [169].

780 **Table 1: Summary of Literature Reports on the Use of nanocluster in Catalysis**

Sl NO	Photocatalyst	Co catalyst	Application	Efficiency	Reference
1	TiO_2-Au NCs@β-CD	AuNC coupled with per-6-thio-β-cyclodextrin (SH-β-CD)	Photodegradation of dyes	98% degradation in 10 minutes of exposure.	[116]
2	Ag/TiO_2/Nb	AgNC stabilized by Captopril	Photodegradation of dyes.	100% degradation	[118]
3	AgNC/CeO_2	AgNC stabilized by Polyethylene imine (PEI)	Photodegradation of dyes.	80% degradation in 2 hours	[119]
4	ZnO–Ag NCs.	AgNC	Photodegradation of dyes.	100% degradation in 1 hr	[120]
5	CuNC: $[Cu_{18}(CH_3COO)(OH)]^{-2}$ and $[Cu_{34}O_2(CH_3COO)_3N(C_4H_9)_3Na]^{-2.}$	No Cocatalyst	Photodegradation of dyes.	100% degradation in 1 69hr	[121]

6	AuNC@MPTS (MPTS-3-Mercaptopropyl trimethoxysilane)	No cocatalyst	Photodegradation of dyes.	100% degradation in 1 hr	[49]
7	(Ag_{12}TPyP)	No cocatalyst	Photodegradation of dyes.	98% degradation	[123]
8	SiO_2-Au GSH clusters-BPEI@TiO_2	SiO_2-Au GSH clusters-BEPI	Photodegradation of organic dyes.	99.1% degradation in 0.5 hr	[124]
9	Au_{25} NC -TiO_2	Au_{25} NC	Oxidation of phenol derivatives and ferrocyanide and reduction of Ag+, Cu2+, and oxygen		[129]
10	Au_{25}NC	No Catalyst	oxidation of styrene and hydrogenation of α,β-unsaturated ketone	27 ± 1.0%	[130]
11	$[Au_{25}(PPh_3)_{10}(SR)_5Cl_2]$-$TiO_2$	AuNC: $[Au_{25}(PPh_3)_{10}(SR)_5Cl_2]$	Oxidation of benzylamines to imines	73-99%	[126]

12	Ag/ZX-Bi_200	Ag NC: (Ag/ZX-Bi_200)	Photooxidation of methanol	49.60 $mmol \cdot g^{-1} \cdot cm^{-2}$ after 12 h of reaction	[132]
13	Aux-GSH NCs @TiO_2	Aux-GSH NCs	Production of H_2	0.3 mmol of hydrogen/h/g	[171]
14	Aux/NP-TNTA NP-TNTAs- TiO_2 nanotube arrays	AuNC	Photodegradation of organic dyes, photocatalytic reduction of aromatic nitro compounds, and photoelectrochemical water splitting.		[136]
15	$(Au_{25}(SG)_{18})$-$BaLa_4Ti_4O_{15}$	AuNC: $(Au_{25}(SG)_{18})$	Photocatalytic water splitting	190 μmol/h	[146]
16	$Au_{25}/SrTiO_3$	AuNC	Hydrogen evolution reaction	41.2 μmol/h of H	[137]
17	Au_{101}NCs -$AlSrTiO_3$ -rGO	Au_{101}NCs	photocatalytic production of H_2, photocatalytic	385 ± 22 nmol h^{-1}	[147]

			water splitting		
18	GNRs-AgNCs GNRS-Gold nanorods	AgNCs	Hydrogen evolution reaction	10%	[138]
19	Pt/ HTi_2NbO_7 Monolayer niobate (HTi_2NbO_7)	Pt NC	Higher H_2 production	10 μmol h^{-1}	[140]
20	Pt_{46}NC-CdS Modified cadmium sulfide (CdS) nanorod	Pt_{46}NC	Photocatalytic water splitting	1.5‰ h^{-1}	[148]
21	Au_{24}Pd NCs -$BaLa_4Ti_4O_{15}$ & Au_{24}Pt NCs- $BaLa_4Ti_4O_{15}$	Au_{24}Pd NCs and Au_{24}Pt NCs	photocatalytic H_2 evolution	100-150 μmolh^{-1}	[149]
22	$PtAg_{24}$ NC-g-C_3N_4	$PtAg_{24}$ NC	photocatalytic H_2 production	39.7 μmolh^{-1}	[142]
23	Cu-BTN -TiO_2	CuNCs: (Cu-BTN)	Photocatalytic CO_2 reduction	150.9 μmol g^{-1} h^{-1}	[167]
24	Metal cations -Fe^{2+},	Au NCs: (Au_c-C-Co)	Photocatalytic	3.45	[168]

	Co^{2+}, Ni^{2+} and Cu^{2+}	& (Au_c-MPA-Co)	CO_2 reduction	$\mu mol \cdot_{great}^{-1} \cdot h^{-1}$	
25	CODH/AgNCs-PMAA/ TiO_2 CODH-carbon monoxide dehydrogenase	Ag NC coupled with PMAA	Photocatalytic CO_2 reduction	turnover frequency of 20 s^{-1}	[172]
26	Au-NCs @MOF		Photocatalytic CO_2 reduction	57.6 μmol $g^{-1}h^{-1}$	[169]
27	Ni-NCs-TiO_2	Ni-NCs	photocatalytic CO_2 reduction	10 μmol g-cat^{-1}	[170]
28	AgNC@ZX-V	No Cocatalyst	reforming of formic acid to H_2 and CO_2	99% selectivity	[173]

5. Conclusion and Future Perspective

MNCs are an under-explored class of nanomaterials with an unimaginable grade of potential. The review summarizes recent progress in the metal nanocluster-based photocatalyst for various photocatalytic reactions, correlating it to their structure and properties to boost single metal, alloy hybrid systems and nanocomposite systems effectiveness. However, research on MNCs has not surpassed the embryonic stage yet. In particular, preventing aggregation, effective capping agents or stabilizers, optical & electronic structures, metal-support bonding, mechanistic learning, in situ characterization techniques, structural model theories, and appreciable yield yearn for more attention. Gold and AgNCs still dominate a major fraction of scientific publications in this domain; works on other transition metals could be more productive and cost-effective. The recyclability of MNCs in photocatalysis with adequate stability after multiple cycles have to be extensively analyzed. At the same time, computer simulations could open the world of possibilities of metal NCs to us, and recent additions to the software have proven their effectiveness. ~~Of note,~~ NCs can plausibly be the answer for low carbon fuels, a milestone to sustainable development and an affordable photocatalyst.

Acknowledgment

Meegle S Mathew thanks the University Grant Commission (UGC)DR DS Kothari Fellowship for financial support. Rodolphe Antoine acknowledges Shanghai Science and Technology Innovation Program (22520712500) for support. In addition, the authors deeply acknowledge French National

Centre for Scientific Research (CNRS) for funding through International Emerging Actions (IEA) between Institut Lumière Matière, CNRS, France, and Mahatma Gandhi University, India.

Reference

1. Fujishima, A.; Honda, K. Electrochemical Photolysis of Water at a Semiconductor Electrode. *Nature* **1972**, *238*, 37–38, doi:10.1038/238037a0.
2. Bakbolat, B.; Daulbayev, C.; Sultanov, F.; Beissenov, R.; Umirzakov, A.; Mereke, A.; Bekbaev, A.; Chuprakov, I. Recent Developments of TiO2-Based Photocatalysis in the Hydrogen Evolution and Photodegradation: A Review. *Nanomaterials* **2020**, *10*, 1790, doi:10.3390/nano10091790.
3. Cheng, L.; Xiang, Q.; Liao, Y.; Zhang, H. CdS-Based Photocatalysts. *Energy Environ. Sci.* **2018**, *11*, 1362–1391, doi:10.1039/C7EE03640J.
4. Ong, C.B.; Ng, L.Y.; Mohammad, A.W. A Review of ZnO Nanoparticles as Solar Photocatalysts: Synthesis, Mechanisms and Applications. *Renewable and Sustainable Energy Reviews* **2018**, *81*, 536–551, doi:10.1016/j.rser.2017.08.020.
5. Hitam, C.N.C.; Jalil, A.A. A Review on Exploration of Fe2O3 Photocatalyst towards Degradation of Dyes and Organic Contaminants. *Journal of Environmental Management* **2020**, *258*, 110050, doi:10.1016/j.jenvman.2019.110050.
6. Lee, G.-J.; Wu, J.J. Recent Developments in ZnS Photocatalysts from Synthesis to Photocatalytic Applications — A Review. *Powder Technology* **2017**, *318*, 8–22, doi:10.1016/j.powtec.2017.05.022.
7. Li, J.; Lou, Z.; Li, B. Nanostructured Materials with Localized Surface Plasmon Resonance for Photocatalysis. *Chinese Chemical Letters* **2022**, *33*, 1154–1168, doi:10.1016/j.cclet.2021.07.059.
8. Song, X.-R.; Goswami, N.; Yang, H.-H.; Xie, J. Functionalization of Metal Nanoclusters for Biomedical Applications. *Analyst* **2016**, *141*, 3126–3140, doi:10.1039/C6AN00773B.
9. Goswami, N.; Zheng, K.; Xie, J. Bio-NCs – the Marriage of Ultrasmall Metal Nanoclusters with Biomolecules. *Nanoscale* **2014**, *6*, 13328–13347, doi:10.1039/C4NR04561K.
10. Basu, S.; Paul, A.; Antoine, R. Controlling the Chemistry of Nanoclusters: From Atomic Precision to Controlled Assembly. *Nanomaterials* **2021**, *12*, 62, doi:10.3390/nano12010062.
11. Wu, Z.; Jin, R. On the Ligand's Role in the Fluorescence of Gold Nanoclusters. *Nano Lett.* **2010**, *10*, 2568–2573, doi:10.1021/nl101225f.
12. Liu, L.; Corma, A. Metal Catalysts for Heterogeneous Catalysis: From Single Atoms to Nanoclusters and Nanoparticles. *Chem. Rev.* **2018**, *118*, 4981–5079, doi:10.1021/acs.chemrev.7b00776.
13. Du, X.; Jin, R. Atomically Precise Metal Nanoclusters for Catalysis. *ACS Nano* **2019**, *13*, 7383–7387, doi:10.1021/acsnano.9b04533.
14. Khandelwal, P.; Poddar, P. Fluorescent Metal Quantum Clusters: An Updated Overview of the Synthesis, Properties, and Biological Applications. *J. Mater. Chem. B* **2017**, *5*, 9055–9084, doi:10.1039/C7TB02320K.
15. Templeton, A.C.; Wuelfing, W.P.; Murray, R.W. Monolayer-Protected Cluster Molecules. *Acc. Chem. Res.* **2000**, *33*, 27–36, doi:10.1021/ar9602664.
16. Qu, X.; Li, Y.; Li, L.; Wang, Y.; Liang, J.; Liang, J. Fluorescent Gold Nanoclusters: Synthesis and Recent Biological Application. *Journal of Nanomaterials* **2015**, *2015*, 1–23, doi:10.1155/2015/784097.
17. Yang, T.-Q.; Peng, B.; Shan, B.-Q.; Zong, Y.-X.; Jiang, J.-G.; Wu, P.; Zhang, K. Origin of the Photoluminescence of Metal Nanoclusters: From Metal-Centered Emission to Ligand-Centered Emission. *Nanomaterials* **2020**, *10*, 261, doi:10.3390/nano10020261.

18. Antoine, R. Supramolecular Gold Chemistry: From Atomically Precise Thiolate-Protected Gold Nanoclusters to Gold-Thiolate Nanostructures. *Nanomaterials* **2020**, *10*, 377, doi:10.3390/nano10020377.
19. Kolay, S.; Bain, D.; Maity, S.; Devi, A.; Patra, A.; Antoine, R. Self-Assembled Metal Nanoclusters: Driving Forces and Structural Correlation with Optical Properties. *Nanomaterials* **2022**, *12*, 544, doi:10.3390/nano12030544.
20. Su, Y.; Xue, T.; Liu, Y.; Qi, J.; Jin, R.; Lin, Z. Luminescent Metal Nanoclusters for Biomedical Applications. *Nano Res.* **2019**, *12*, 1251–1265, doi:10.1007/s12274-019-2314-y.
21. Bonačić-Koutecký, V.; Antoine, R. Enhanced Two-Photon Absorption of Ligated Silver and Gold Nanoclusters: Theoretical and Experimental Assessments. *Nanoscale* **2019**, *11*, 12436–12448, doi:10.1039/C9NR01826C.
22. Genji Srinivasulu, Y.; Yao, Q.; Goswami, N.; Xie, J. Interfacial Engineering of Gold Nanoclusters for Biomedical Applications. *Mater. Horiz.* **2020**, *7*, 2596–2618, doi:10.1039/D0MH00827C.
23. Antoine, R.; Maysinger, D.; Sancey, L.; Bonačić-Koutecký, V. Open Questions on Proteins Interacting with Nanoclusters. *Commun Chem* **2022**, *5*, 47, doi:10.1038/s42004-022-00665-9.
24. Combes, G.F.; Vučković, A.-M.; Perić Bakulić, M.; Antoine, R.; Bonačić-Koutecky, V.; Trajković, K. Nanotechnology in Tumor Biomarker Detection: The Potential of Liganded Nanoclusters as Nonlinear Optical Contrast Agents for Molecular Diagnostics of Cancer. *Cancers* **2021**, *13*, 4206, doi:10.3390/cancers13164206.
25. Rudzińska, M.; Daglioglu, C.; Savvateeva, L.V.; Kaci, F.N.; Antoine, R.; Zamyatnin Jr, A.A. Current Status and Perspectives of Protease Inhibitors and Their Combination with Nanosized Drug Delivery Systems for Targeted Cancer Therapy. *DDDT* **2021**, *Volume 15*, 9–20, doi:10.2147/DDDT.S285852.
26. Borghei, Y.; Hosseinkhani, S.; Ganjali, M.R. Bridging from Metallic Nanoclusters to Biomedical in Understanding Physicochemical Interactions at the Nano–Bio Interface. *Part & Part Syst Charact* **2022**, *39*, 2100202, doi:10.1002/ppsc.202100202.
27. Chai, O.J.H.; Liu, Z.; Chen, T.; Xie, J. Engineering Ultrasmall Metal Nanoclusters for Photocatalytic and Electrocatalytic Applications. *Nanoscale* **2019**, *11*, 20437–20448, doi:10.1039/C9NR07272A.
28. Liang, H.; Liu, B.-J.; Tang, B.; Zhu, S.-C.; Li, S.; Ge, X.-Z.; Li, J.-L.; Zhu, J.-R.; Xiao, F.-X. Atomically Precise Metal Nanocluster-Mediated Photocatalysis. *ACS Catal.* **2022**, *12*, 4216–4226, doi:10.1021/acscatal.2c00841.
29. Munir, A.; Joya, K.S.; Ul haq, T.; Babar, N.; Hussain, S.Z.; Qurashi, A.; Ullah, N.; Hussain, I. Metal Nanoclusters: New Paradigm in Catalysis for Water Splitting, Solar and Chemical Energy Conversion. *ChemSusChem* **2019**, *12*, 1517–1548, doi:10.1002/cssc.201802069.
30. Kauffman, D.R.; Thakkar, J.; Siva, R.; Matranga, C.; Ohodnicki, P.R.; Zeng, C.; Jin, R. Efficient Electrochemical CO 2 Conversion Powered by Renewable Energy. *ACS Appl. Mater. Interfaces* **2015**, *7*, 15626–15632, doi:10.1021/acsami.5b04393.
31. Al Dosari, H.M.; Ayesh, A.I. Nanocluster Production for Solar Cell Applications. *Journal of Applied Physics* **2013**, *114*, 054305, doi:10.1063/1.4817421.
32. Fang, J.; Zhang, B.; Yao, Q.; Yang, Y.; Xie, J.; Yan, N. Recent Advances in the Synthesis and Catalytic Applications of Ligand-Protected, Atomically Precise Metal Nanoclusters. *Coordination Chemistry Reviews* **2016**, *322*, 1–29, doi:10.1016/j.ccr.2016.05.003.
33. Serhan, M.; Jackemeyer, D.; Long, M.; Sprowls, M.; Diez Perez, I.; Maret, W.; Chen, F.; Tao, N.; Forzani, E. Total Iron Measurement in Human Serum With a Novel Smartphone-Based Assay. *IEEE J. Transl. Eng. Health Med.* **2020**, *8*, 1–9, doi:10.1109/JTEHM.2020.3005308.
34. Yao, Q.; Yuan, X.; Chen, T.; Leong, D.T.; Xie, J. Engineering Functional Metal Materials at the Atomic Level. *Adv. Mater.* **2018**, *30*, 1802751, doi:10.1002/adma.201802751.

35. Mathew, A.; Pradeep, T. Noble Metal Clusters: Applications in Energy, Environment, and Biology. *Part. Part. Syst. Charact.* **2014**, *31*, 1017–1053, doi:10.1002/ppsc.201400033.
36. Jadzinsky, P.D.; Calero, G.; Ackerson, C.J.; Bushnell, D.A.; Kornberg, R.D. Structure of a Thiol Monolayer-Protected Gold Nanoparticle at 1.1 Å Resolution. *Science* **2007**, *318*, 430–433, doi:10.1126/science.1148624.
37. Qian, H.; Eckenhoff, W.T.; Zhu, Y.; Pintauer, T.; Jin, R. Total Structure Determination of Thiolate-Protected Au_{38} Nanoparticles. *J. Am. Chem. Soc.* **2010**, *132*, 8280–8281, doi:10.1021/ja103592z.
38. Zeng, C.; Qian, H.; Li, T.; Li, G.; Rosi, N.L.; Yoon, B.; Barnett, R.N.; Whetten, R.L.; Landman, U.; Jin, R. Total Structure and Electronic Properties of the Gold Nanocrystal $Au_{36}(SR)_{24}$. *Angew. Chem. Int. Ed.* **2012**, *51*, 13114–13118, doi:10.1002/anie.201207098.
39. Das, A.; Li, T.; Nobusada, K.; Zeng, Q.; Rosi, N.L.; Jin, R. Total Structure and Optical Properties of a Phosphine/Thiolate-Protected Au_{24} Nanocluster. *J. Am. Chem. Soc.* **2012**, *134*, 20286–20289, doi:10.1021/ja3101566.
40. Zeng, C.; Li, T.; Das, A.; Rosi, N.L.; Jin, R. Chiral Structure of Thiolate-Protected 28-Gold-Atom Nanocluster Determined by X-Ray Crystallography. *J. Am. Chem. Soc.* **2013**, *135*, 10011–10013, doi:10.1021/ja404058q.
41. Jin, R.; Zeng, C.; Zhou, M.; Chen, Y. Atomically Precise Colloidal Metal Nanoclusters and Nanoparticles: Fundamentals and Opportunities. *Chem. Rev.* **2016**, *116*, 10346–10413, doi:10.1021/acs.chemrev.5b00703.
42. Lu, Y.; Chen, W. Application of Mass Spectrometry in the Synthesis and Characterization of Metal Nanoclusters. *Anal. Chem.* **2015**, *87*, 10659–10667, doi:10.1021/acs.analchem.5b00848.
43. Chakraborty, P.; Pradeep, T. The Emerging Interface of Mass Spectrometry with Materials. *NPG Asia Mater* **2019**, *11*, 48, doi:10.1038/s41427-019-0149-3.
44. Comby-Zerbino, C.; Dagany, X.; Chirot, F.; Dugourd, P.; Antoine, R. The Emergence of Mass Spectrometry for Characterizing Nanomaterials. Atomically Precise Nanoclusters and Beyond. *Mater. Adv.* **2021**, *2*, 4896–4913, doi:10.1039/D1MA00261A.
45. Zhao, Y.; Zhou, H.; Zhang, S.; Xu, J. The Synthesis of Metal Nanoclusters and Their Applications in Bio-Sensing and Imaging. *Methods Appl. Fluoresc.* **2019**, *8*, 012001, doi:10.1088/2050-6120/ab57e7.
46. Liu, Z.; Wu, Z.; Yao, Q.; Cao, Y.; Chai, O.J.H.; Xie, J. Correlations between the Fundamentals and Applications of Ultrasmall Metal Nanoclusters: Recent Advances in Catalysis and Biomedical Applications. *Nano Today* **2021**, *36*, 101053, doi:10.1016/j.nantod.2020.101053.
47. Ling, S.; Cui, X.; Zhang, X.; Liu, B.; He, C.; Wang, J.; Qin, W.; Zhang, Y.; Gao, Y.; Bai, G. Glutathione-Protected Gold Nanocluster Decorated Cadmium Sulfide with Enhanced Photostability and Photocatalytic Activity. *Journal of Colloid and Interface Science* **2018**, *530*, 120–126, doi:10.1016/j.jcis.2018.06.055.
48. Mathew, M.S.; Joseph, K. Green Synthesis of Gluten-Stabilized Fluorescent Gold Quantum Clusters: Application As Turn-On Sensing of Human Blood Creatinine. *ACS Sustainable Chem. Eng.* **2017**, *5*, 4837–4845, doi:10.1021/acssuschemeng.7b00273.
49. Zhou, S.; Duan, Y.; Wang, F.; Wang, C. Fluorescent Au Nanoclusters Stabilized by Silane: Facile Synthesis, Color-Tunability and Photocatalytic Properties. *Nanoscale* **2017**, *9*, 4981–4988, doi:10.1039/C7NR01052D.
50. Li, Y.; Zaluzhna, O.; Xu, B.; Gao, Y.; Modest, J.M.; Tong, Y.J. Mechanistic Insights into the Brust−Schiffrin Two-Phase Synthesis of Organo-Chalcogenate-Protected Metal Nanoparticles. *J. Am. Chem. Soc.* **2011**, *133*, 2092–2095, doi:10.1021/ja1105078.

51. Dhanalakshmi, L.; Udayabhaskararao, T.; Pradeep, T. Conversion of Double Layer Charge-Stabilized Ag@citrate Colloids to Thiol Passivated Luminescent Quantum Clusters. *Chem. Commun.* **2012**, *48*, 859–861, doi:10.1039/C1CC15604G.
52. Zhu, L.; Gharib, M.; Becker, C.; Zeng, Y.; Ziefuß, A.R.; Chen, L.; Alkilany, A.M.; Rehbock, C.; Barcikowski, S.; Parak, W.J.; et al. Synthesis of Fluorescent Silver Nanoclusters: Introducing Bottom-Up and Top-Down Approaches to Nanochemistry in a Single Laboratory Class. *J. Chem. Educ.* **2020**, *97*, 239–243, doi:10.1021/acs.jchemed.9b00342.
53. Meng, X.; Xu, Q.; Wang, S.; Zhu, M. Ligand-Exchange Synthesis of Selenophenolate-Capped Au25 Nanoclusters. *Nanoscale* **2012**, *4*, 4161, doi:10.1039/c2nr30272a.
54. Wang, Y.; Bürgi, T. Ligand Exchange Reactions on Thiolate-Protected Gold Nanoclusters. *Nanoscale Adv.* **2021**, *3*, 2710–2727, doi:10.1039/D1NA00178G.
55. Heinecke, C.L.; Ni, T.W.; Malola, S.; Mäkinen, V.; Wong, O.A.; Häkkinen, H.; Ackerson, C.J. Structural and Theoretical Basis for Ligand Exchange on Thiolate Monolayer Protected Gold Nanoclusters. *J. Am. Chem. Soc.* **2012**, *134*, 13316–13322, doi:10.1021/ja3032339.
56. Udaya Bhaskara Rao, T.; Pradeep, T. Luminescent Ag7 and Ag8 Clusters by Interfacial Synthesis. *Angewandte Chemie International Edition* **2010**, *49*, 3925–3929, doi:10.1002/anie.200907120.
57. Bootharaju, M.S.; Burlakov, V.M.; Besong, T.M.D.; Joshi, C.P.; AbdulHalim, L.G.; Black, D.M.; Whetten, R.L.; Goriely, A.; Bakr, O.M. Reversible Size Control of Silver Nanoclusters via Ligand-Exchange. *Chem. Mater.* **2015**, *27*, 4289–4297, doi:10.1021/acs.chemmater.5b00650.
58. Antonello, S.; Dainese, T.; Pan, F.; Rissanen, K.; Maran, F. Electrocrystallization of Monolayer-Protected Gold Clusters: Opening the Door to Quality, Quantity, and New Structures. *J. Am. Chem. Soc.* **2017**, *139*, 4168–4174, doi:10.1021/jacs.7b00568.
59. Brust, M.; Walker, M.; Bethell, D.; Schiffrin, D.J.; Whyman, R. Synthesis of Thiol-Derivatised Gold Nanoparticles in a Two-Phase Liquid–Liquid System. *J. Chem. Soc., Chem. Commun.* **1994**, *0*, 801–802, doi:10.1039/C39940000801.
60. Negishi, Y.; Nobusada, K.; Tsukuda, T. Glutathione-Protected Gold Clusters Revisited: Bridging the Gap between Gold(I)−Thiolate Complexes and Thiolate-Protected Gold Nanocrystals. *J. Am. Chem. Soc.* **2005**, *127*, 5261–5270, doi:10.1021/ja042218h.
61. Chen, S.; Templeton, A.C.; Murray, R.W. Monolayer-Protected Cluster Growth Dynamics. *Langmuir* **2000**, *16*, 3543–3548, doi:10.1021/la991206k.
62. Edinger, K.; Goelzhaeuser, A.; Demota, K.; Woell, C.; Grunze, M. Formation of Self-Assembled Monolayers of n-Alkanethiols on Gold: A Scanning Tunneling Microscopy Study on the Modification of Substrate Morphology. *Langmuir* **1993**, *9*, 4–8, doi:10.1021/la00025a002.
63. Habeeb Muhammed, M.A.; Ramesh, S.; Sinha, S.S.; Pal, S.K.; Pradeep, T. Two Distinct Fluorescent Quantum Clusters of Gold Starting from Metallic Nanoparticles by PH-Dependent Ligand Etching. *Nano Res.* **2008**, *1*, 333–340, doi:10.1007/s12274-008-8035-2.
64. Yuan, X.; Luo, Z.; Zhang, Q.; Zhang, X.; Zheng, Y.; Lee, J.Y.; Xie, J. Synthesis of Highly Fluorescent Metal (Ag, Au, Pt, and Cu) Nanoclusters by Electrostatically Induced Reversible Phase Transfer. *ACS Nano* **2011**, *5*, 8800–8808, doi:10.1021/nn202860s.
65. Thomas, S. *Luminescent Metal Nanoclusters: Synthesis, Characterisation and Applications*; Woodhead Publishing: Cambridge, 2022; ISBN 978-0-323-88641-3.

964 66. *Atomic Clusters: From Gas Phase to Deposited*; Woodruff, D.P., Ed.; The chemical physics of solid surfaces; 1st ed.;
965 Elsevier: Amsterdam ; Boston, 2007; ISBN 978-0-444-52756-1.
966 67. Briant, C.E.; Theobald, B.R.C.; White, J.W.; Bell, L.K.; Mingos, D.M.P.; Welch, A.J. Synthesis and X-Ray
967 Structural Characterization of the Centred Icosahedral Gold Cluster Compound [Aul3(PMe2Ph)10Cl2](PF6)3;
968 the Realization of a Theoretical Prediction. *J. Chem. Soc., Chem. Commun.* **1981**, 201, doi:10.1039/c39810000201.
969 68. Akola, J.; Walter, M.; Whetten, R.L.; Häkkinen, H.; Grönbeck, H. On the Structure of Thiolate-Protected Au_{25}. *J.*
970 *Am. Chem. Soc.* **2008**, *130*, 3756–3757, doi:10.1021/ja800594p.
971 69. Xavier, P.L.; Chaudhari, K.; Baksi, A.; Pradeep, T. Protein-Protected Luminescent Noble Metal Quantum
972 Clusters: An Emerging Trend in Atomic Cluster Nanoscience. *Nano Reviews* **2012**, *3*, 14767,
973 doi:10.3402/nano.v3i0.14767.
974 70. Alex, A.M.; Mathew, M.S.; Kuruvilla, K.J.; Appukuttan, S.; Joseph, K.; Thomas, S. Protein and Enzyme
975 Protected Metal Nanoclusters. In *Luminescent Metal Nanoclusters*; Elsevier, 2022; pp. 303–348 ISBN
976 978-0-323-88657-4.
977 71. Halawa, M.I.; Lai, J.; Xu, G. Gold Nanoclusters: Synthetic Strategies and Recent Advances in Fluorescent
978 Sensing. *Materials Today Nano* **2018**, *3*, 9–27, doi:10.1016/j.mtnano.2018.11.001.
979 72. Chen, L.-Y.; Wang, C.-W.; Yuan, Z.; Chang, H.-T. Fluorescent Gold Nanoclusters: Recent Advances in Sensing
980 and Imaging. *Anal. Chem.* **2015**, *87*, 216–229, doi:10.1021/ac503636j.
981 73. Hayyan, M.; Hashim, M.A.; AlNashef, I.M. Superoxide Ion: Generation and Chemical Implications. *Chem. Rev.*
982 **2016**, *116*, 3029–3085, doi:10.1021/acs.chemrev.5b00407.
983 74. Xie, J.; Zheng, Y.; Ying, J.Y. Protein-Directed Synthesis of Highly Fluorescent Gold Nanoclusters. *J. Am. Chem.*
984 *Soc.* **2009**, *131*, 888–889, doi:10.1021/ja806804u.
985 75. Le Guével, X.; Hötzer, B.; Jung, G.; Hollemeyer, K.; Trouillet, V.; Schneider, M. Formation of Fluorescent Metal
986 (Au, Ag) Nanoclusters Capped in Bovine Serum Albumin Followed by Fluorescence and Spectroscopy. *J. Phys.*
987 *Chem. C* **2011**, *115*, 10955–10963, doi:10.1021/jp111820b.
988 76. Stamplecoskie, K.G.; Swint, A. Optimizing Molecule-like Gold Clusters for Light Energy Conversion. *J. Mater.*
989 *Chem. A* **2016**, *4*, 2075–2081, doi:10.1039/C5TA07580G.
990 77. Robinson, D. Synthesis and Characterization of Metal Nanoclusters Stabilized by Dithiolates.,
991 doi:10.57709/2171175.
992 78. Kreibig, U.; Vollmer, M. *Optical Properties of Metal Clusters*; Springer Series in Materials Science; Springer Berlin
993 Heidelberg: Berlin, Heidelberg, 1995; Vol. 25; ISBN 978-3-642-08191-0.
994 79. Antoine, R.; Bonačić-Koutecký, V. *Liganded Silver and Gold Quantum Clusters. Towards a New Class of Nonlinear*
995 *Optical Nanomaterials*; SpringerBriefs in Materials; Springer International Publishing: Cham, 2018; ISBN
996 978-3-319-64742-5.
997 80. Jin, R.; Higaki, T. Open Questions on the Transition between Nanoscale and Bulk Properties of Metals.
998 *Commun Chem* **2021**, *4*, 28, doi:10.1038/s42004-021-00466-6.
999 81. Huang, X.; Li, Z.; Yu, Z.; Deng, X.; Xin, Y. Recent Advances in the Synthesis, Properties, and Biological
1000 Applications of Platinum Nanoclusters. *Journal of Nanomaterials* **2019**, *2019*, 1–31, doi:10.1155/2019/6248725.
1001 82. Muhammed, M.A.H.; Verma, P.K.; Pal, S.K.; Kumar, R.C.A.; Paul, S.; Omkumar, R.V.; Pradeep, T. Bright,
1002 NIR-Emitting Au_{23} from Au_{25} : Characterization and Applications Including Biolabeling. *Chem. Eur. J.* **2009**, *15*,
1003 10110–10120, doi:10.1002/chem.200901425.

83. Zhu, M.; Aikens, C.M.; Hollander, F.J.; Schatz, G.C.; Jin, R. Correlating the Crystal Structure of A Thiol-Protected Au $_{25}$ Cluster and Optical Properties. *J. Am. Chem. Soc.* **2008**, *130*, 5883–5885, doi:10.1021/ja801173r.
84. Du, Y.; Sheng, H.; Astruc, D.; Zhu, M. Atomically Precise Noble Metal Nanoclusters as Efficient Catalysts: A Bridge between Structure and Properties. *Chem. Rev.* **2020**, *120*, 526–622, doi:10.1021/acs.chemrev.8b00726.
85. Li, S.; Du, X.; Liu, Z.; Li, Y.; Shao, Y.; Jin, R. Size Effects of Atomically Precise Gold Nanoclusters in Catalysis. *Precision Chemistry* **2023**, *1*, 14–28, doi:10.1021/prechem.3c00008.
86. Shang, L.; Dong, S.; Nienhaus, G.U. Ultra-Small Fluorescent Metal Nanoclusters: Synthesis and Biological Applications. *Nano Today* **2011**, *6*, 401–418, doi:10.1016/j.nantod.2011.06.004.
87. Bertorelle, F.; Wegner, D.; Bakulić, M.P.; Fakhouri, H.; Comby-Zerbino, C.; Sagar, A.; Bernadó, P.; Resch-Genger, U.; Koutecky, V.B.; Guével, X.L.; et al. *Tailoring NIR-II Photoluminescence of Single Thiolated Au25 Nanoclusters by Selective Binding to Proteins*; In Review, 2021;
88. Tang, J.-H.; Han, G.; Li, G.; Yan, K.; Sun, Y. Near-Infrared Light Photocatalysis Enabled by a Ruthenium Complex-Integrated Metal–Organic Framework via Two-Photon Absorption. *iScience* **2022**, *25*, 104064, doi:10.1016/j.isci.2022.104064.
89. Russier-Antoine, I.; Bertorelle, F.; Calin, N.; Sanader, Ž.; Krstić, M.; Comby-Zerbino, C.; Dugourd, P.; Brevet, P.-F.; Bonačić-Koutecký, V.; Antoine, R. Ligand-Core NLO-Phores: A Combined Experimental and Theoretical Approach to the Two-Photon Absorption and Two-Photon Excited Emission Properties of Small-Ligated Silver Nanoclusters. *Nanoscale* **2017**, *9*, 1221–1228, doi:10.1039/C6NR07989J.
90. Antoine, R. Ligand-Core NLO-Phores: Two-Photon Absorption and Two-Photon Excited Emission Properties of Atomically Precise Clusters of Gold and Silver. In *Molecular Spectroscopy—Experiment and Theory*; Koleżyński, A., Król, M., Eds.; Challenges and Advances in Computational Chemistry and Physics; Springer International Publishing: Cham, 2019; Vol. 26, pp. 139–160 ISBN 978-3-030-01354-7.
91. Sanader, Ž.; Krstić, M.; Russier-Antoine, I.; Bertorelle, F.; Dugourd, P.; Brevet, P.-F.; Antoine, R.; Bonačić-Koutecký, V. Two-Photon Absorption of Ligand-Protected Ag $_{15}$ Nanoclusters. Towards a New Class of Nonlinear Optics Nanomaterials. *Phys. Chem. Chem. Phys.* **2016**, *18*, 12404–12408, doi:10.1039/C6CP00207B.
92. Hao, C.; Xu, L.; Ma, W.; Wu, X.; Wang, L.; Kuang, H.; Xu, C. Unusual Circularly Polarized Photocatalytic Activity in Nanogapped Gold-Silver Chiroplasmonic Nanostructures. *Adv. Funct. Mater.* **2015**, *25*, 5816–5822, doi:10.1002/adfm.201502429.
93. Schaaff, T.G.; Knight, G.; Shafigullin, M.N.; Borkman, R.F.; Whetten, R.L. Isolation and Selected Properties of a 10.4 KDa Gold:Glutathione Cluster Compound. *J. Phys. Chem. B* **1998**, *102*, 10643–10646, doi:10.1021/jp9830528.
94. Yao, H. Chiral Ligand-Protected Gold Nanoclusters: Considering the Optical Activity from a Viewpoint of Ligand Dissymmetric Field. *Progress in Natural Science: Materials International* **2016**, *26*, 428–439, doi:10.1016/j.pnsc.2016.08.006.
95. Tsukuda, T.; Häkkinen, H. Introduction. In *Frontiers of Nanoscience*; Elsevier, 2015; Vol. 9, pp. 1–7 ISBN 978-0-08-100086-1.
96. Shichibu, Y.; Negishi, Y.; Tsunoyama, H.; Kanehara, M.; Teranishi, T.; Tsukuda, T. Extremely High Stability of Glutathionate-Protected Au25 Clusters Against Core Etching. *Small* **2007**, *3*, 835–839, doi:10.1002/smll.200600611.
97. Boyen, H.-G.; Kästle, G.; Weigl, F.; Koslowski, B.; Dietrich, C.; Ziemann, P.; Spatz, J.P.; Riethmüller, S.; Hartmann, C.; Möller, M.; et al. Oxidation-Resistant Gold-55 Clusters. *Science* **2002**, *297*, 1533–1536, doi:10.1126/science.1076248.

98. Tracy, J.B.; Kalyuzhny, G.; Crowe, M.C.; Balasubramanian, R.; Choi, J.-P.; Murray, R.W. Poly(Ethylene Glycol) Ligands for High-Resolution Nanoparticle Mass Spectrometry. *J. Am. Chem. Soc.* **2007**, *129*, 6706–6707, doi:10.1021/ja071042r.
99. Kumar, S.; Jin, R. Water-Soluble Au25(Capt)18 Nanoclusters: Synthesis, Thermal Stability, and Optical Properties. *Nanoscale* **2012**, *4*, 4222, doi:10.1039/c2nr30833a.
100. Negishi, Y.; Kurashige, W.; Niihori, Y.; Iwasa, T.; Nobusada, K. Isolation, Structure, and Stability of a Dodecanethiolate-Protected Pd1Au24 Cluster. *Phys. Chem. Chem. Phys.* **2010**, *12*, 6219, doi:10.1039/b927175a.
101. Fakhouri, H.; Salmon, E.; Wei, X.; Joly, S.; Moulin, C.; Russier-Antoine, I.; Brevet, P.-F.; Kang, X.; Zhu, M.; Antoine, R. Effects of Single Platinum Atom Doping on Stability and Nonlinear Optical Properties of Ag $_{29}$ Nanoclusters. *J. Phys. Chem. C* **2022**, *126*, 21094–21100, doi:10.1021/acs.jpcc.2c06836.
102. Jiang, D.; Dai, S. From Superatomic Au $_{25}$ (SR) $_{18}^{-}$ to Superatomic M@Au $_{24}$ (SR) $_{18}^{q}$ Core–Shell Clusters. *Inorg. Chem.* **2009**, *48*, 2720–2722, doi:10.1021/ic8024588.
103. Negishi, Y.; Munakata, K.; Ohgake, W.; Nobusada, K. Effect of Copper Doping on Electronic Structure, Geometric Structure, and Stability of Thiolate-Protected Au $_{25}$ Nanoclusters. *J. Phys. Chem. Lett.* **2012**, *3*, 2209–2214, doi:10.1021/jz300892w.
104. Tlahuice-Flores, A.; Muñoz-Castro, A. Bonding and Properties of Superatoms. Analogs to Atoms and Molecules and Related Concepts from Superatomic Clusters. *Int J Quantum Chem* **2019**, *119*, e25756, doi:10.1002/qua.25756.
105. De Heer, W.A.; Knight, W.D.; Chou, M.Y.; Cohen, M.L. Electronic Shell Structure and Metal Clusters. In *Solid State Physics*; Elsevier, 1987; Vol. 40, pp. 93–181 ISBN 978-0-12-607740-7.
106. Bertorelle, F.; Russier-Antoine, I.; Comby-Zerbino, C.; Chirot, F.; Dugourd, P.; Brevet, P.-F.; Antoine, R. Isomeric Effect of Mercaptobenzoic Acids on the Synthesis, Stability, and Optical Properties of Au $_{25}$ (MBA) $_{18}$ Nanoclusters. *ACS Omega* **2018**, *3*, 15635–15642, doi:10.1021/acsomega.8b02615.
107. Sakai, N.; Tatsuma, T. Photovoltaic Properties of Glutathione-Protected Gold Clusters Adsorbed on TiO $_{2}$ Electrodes. *Adv. Mater.* **2010**, *22*, 3185–3188, doi:10.1002/adma.200904317.
108. Wang, H.; Liu, X.; Yang, W.; Mao, G.; Meng, Z.; Wu, Z.; Jiang, H.-L. Surface-Clean Au $_{25}$ Nanoclusters in Modulated Microenvironment Enabled by Metal–Organic Frameworks for Enhanced Catalysis. *J. Am. Chem. Soc.* **2022**, *144*, 22008–22017, doi:10.1021/jacs.2c09136.
109. Duan, Y.; Luo, J.; Zhou, S.; Mao, X.; Shah, M.W.; Wang, F.; Chen, Z.; Wang, C. TiO2-Supported Ag Nanoclusters with Enhanced Visible Light Activity for the Photocatalytic Removal of NO. *Applied Catalysis B: Environmental* **2018**, *234*, 206–212, doi:10.1016/j.apcatb.2018.04.041.
110. Yu, C.; Li, G.; Kumar, S.; Kawasaki, H.; Jin, R. Stable Au $_{25}$ (SR) $_{18}$ /TiO $_{2}$ Composite Nanostructure with Enhanced Visible Light Photocatalytic Activity. *J. Phys. Chem. Lett.* **2013**, *4*, 2847–2852, doi:10.1021/jz401447w.
111. Das, K.; Roychoudhury, A. Reactive Oxygen Species (ROS) and Response of Antioxidants as ROS-Scavengers during Environmental Stress in Plants. *Front. Environ. Sci.* **2014**, *2*, doi:10.3389/fenvs.2014.00053.
112. Sacco, O.; Stoller, M.; Vaiano, V.; Ciambelli, P.; Chianese, A.; Sannino, D. Photocatalytic Degradation of Organic Dyes under Visible Light on N-Doped TiO 2 Photocatalysts. *International Journal of Photoenergy* **2012**, *2012*, 1–8, doi:10.1155/2012/626759.
113. Guo, W.; Yang, L.; Lu, J.; Gao, P.; Li, W.; Feng, Z. An Accurate Growth Mechanism and Photocatalytic Degradation Rhodamine B of Crystalline Nb2O5 Nanotube Arrays. *Catalysts* **2020**, *10*, 1480, doi:10.3390/catal10121480.

114. Goswami, T.; Singh, M.; Reddy, K.M.; Mishra, A.K. Facile Synthesis of Ag-TiO 2 Hybrid Nanocluster:A Comprehensive Experimental and Computational Insight into the Role of Surface Ligands on Enhanced Visible Light Photo-Catalysis. *ChemistrySelect* **2018**, *3*, 10892–10899, doi:10.1002/slct.201801903.
115. Yang, J.; Wang, D.; Han, H.; Li, C. Roles of Cocatalysts in Photocatalysis and Photoelectrocatalysis. *Acc. Chem. Res.* **2013**, *46*, 1900–1909, doi:10.1021/ar300227e.
116. Zhu, H.; Goswami, N.; Yao, Q.; Chen, T.; Liu, Y.; Xu, Q.; Chen, D.; Lu, J.; Xie, J. Cyclodextrin–Gold Nanocluster Decorated TiO 2 Enhances Photocatalytic Decomposition of Organic Pollutants. *J. Mater. Chem. A* **2018**, *6*, 1102–1108, doi:10.1039/C7TA09443D.
117. Sharma, V.; Kumar, S.; Krishnan, V. Clustered Au on TiO 2 Snowman-Like Nanoassemblies for Photocatalytic Applications. *ChemistrySelect* **2016**, *1*, 2963–2970, doi:10.1002/slct.201600671.
118. Goswami, T.; Reddy, K.M.; Bheemaraju, A. Silver Nanocluster Anchored TiO 2 /Nb 2 O 5 Hybrid Nanocomposite as Highly Efficient and Selective Visible-Light Sensitive Photocatalyst. *ChemistrySelect* **2019**, *4*, 6790–6799, doi:10.1002/slct.201901097.
119. Samai, B.; Chall, S.; Mati, S.S.; Bhattacharya, S.C. Role of Silver Nanoclusters in the Enhanced Photocatalytic Activity of Cerium Oxide Nanoparticles. *Eur. J. Inorg. Chem.* **2018**, *2018*, 3224–3231, doi:10.1002/ejic.201800230.
120. González-Rodríguez, J.; Fernández, L.; Bava, Y.B.; Buceta, D.; Vázquez-Vázquez, C.; López-Quintela, M.A.; Feijoo, G.; Moreira, M.T. Enhanced Photocatalytic Activity of Semiconductor Nanocomposites Doped with Ag Nanoclusters Under UV and Visible Light. *Catalysts* **2019**, *10*, 31, doi:10.3390/catal10010031.
121. Vilar-Vidal, N.; Rey, J.R.; López Quintela, M.A. Green Emitter Copper Clusters as Highly Efficient and Reusable Visible Degradation Photocatalysts. *Small* **2014**, *10*, 3632–3636, doi:10.1002/smll.201400679.
122. Veziroglu, S.; Obermann, A.-L.; Ullrich, M.; Hussain, M.; Kamp, M.; Kienle, L.; Leißner, T.; Rubahn, H.-G.; Polonskyi, O.; Strunskus, T.; et al. Photodeposition of Au Nanoclusters for Enhanced Photocatalytic Dye Degradation over TiO 2 Thin Film. *ACS Appl. Mater. Interfaces* **2020**, *12*, 14983–14992, doi:10.1021/acsami.9b18817.
123. Cao, M.; Pang, R.; Wang, Q.-Y.; Han, Z.; Wang, Z.-Y.; Dong, X.-Y.; Li, S.-F.; Zang, S.-Q.; Mak, T.C.W. Porphyrinic Silver Cluster Assembled Material for Simultaneous Capture and Photocatalysis of Mustard-Gas Simulant. *J. Am. Chem. Soc.* **2019**, *141*, 14505–14509, doi:10.1021/jacs.9b05952.
124. Weng, B.; Lu, K.-Q.; Tang, Z.; Chen, H.M.; Xu, Y.-J. Stabilizing Ultrasmall Au Clusters for Enhanced Photoredox Catalysis. *Nat Commun* **2018**, *9*, 1543, doi:10.1038/s41467-018-04020-2.
125. Al-Shankiti, B.; Al-Maksoud, W.; Habeeb Muhammed, M.A.; Anjum, D.H.; Moosa, B.; Basset, J.-M.; Khashab, N.M. Ligand-Free Gold Nanoclusters Confined in Mesoporous Silica Nanoparticles for Styrene Epoxidation. *Nanoscale Adv.* **2020**, *2*, 1437–1442, doi:10.1039/C9NA00781D.
126. Chen, H.; Liu, C.; Wang, M.; Zhang, C.; Luo, N.; Wang, Y.; Abroshan, H.; Li, G.; Wang, F. Visible Light Gold Nanocluster Photocatalyst: Selective Aerobic Oxidation of Amines to Imines. *ACS Catal.* **2017**, *7*, 3632–3638, doi:10.1021/acscatal.6b03509.
127. Liu, L.; Li, H.; Tan, Y.; Chen, X.; Lin, R.; Yang, W.; Huang, C.; Wang, S.; Wang, X.; Liu, X.Y.; et al. Metal-Support Synergy of Supported Gold Nanoclusters in Selective Oxidation of Alcohols. *Catalysts* **2020**, *10*, 107, doi:10.3390/catal10010107.
128. Haruta, M.; Kobayashi, T.; Sano, H.; Yamada, N. Novel Gold Catalysts for the Oxidation of Carbon Monoxide at a Temperature Far Below 0 °C. *Chem. Lett.* **1987**, *16*, 405–408, doi:10.1246/cl.1987.405.
129. Kogo, A.; Sakai, N.; Tatsuma, T. Photocatalysis of Au25-Modified TiO2 under Visible and near Infrared Light. *Electrochemistry Communications* **2010**, *12*, 996–999, doi:10.1016/j.elecom.2010.05.021.

130. Zhu, Y.; Qian, H.; Zhu, M.; Jin, R. Thiolate-Protected Aun Nanoclusters as Catalysts for Selective Oxidation and Hydrogenation Processes. *Adv. Mater.* **2010**, *22*, 1915–1920, doi:10.1002/adma.200903934.
131. Tsunoyama, H.; Ichikuni, N.; Sakurai, H.; Tsukuda, T. Effect of Electronic Structures of Au Clusters Stabilized by Poly(*N* -Vinyl-2-Pyrrolidone) on Aerobic Oxidation Catalysis. *J. Am. Chem. Soc.* **2009**, *131*, 7086–7093, doi:10.1021/ja810045y.
132. Hamoud, H.I.; Douma, F.; Lafjah, M.; Djafri, F.; Lebedev, O.; Valtchev, V.; El-Roz, M. Size-Dependent Photocatalytic Activity of Silver Nanoparticles Embedded in ZX-Bi Zeolite Supports. *ACS Appl. Nano Mater.* **2022**, *5*, 3866–3877, doi:10.1021/acsanm.1c04484.
133. Jain, I.P. Hydrogen the Fuel for 21st Century. *International Journal of Hydrogen Energy* **2009**, *34*, 7368–7378, doi:10.1016/j.ijhydene.2009.05.093.
134. Ahluwalia, R.K.; Wang, X.; Rousseau, A.; Kumar, R. Fuel Economy of Hydrogen Fuel Cell Vehicles. *Journal of Power Sources* **2004**, *130*, 192–201, doi:10.1016/j.jpowsour.2003.12.061.
135. Thoi, V.S.; Sun, Y.; Long, J.R.; Chang, C.J. Complexes of Earth-Abundant Metals for Catalytic Electrochemical Hydrogen Generation under Aqueous Conditions. *Chem. Soc. Rev.* **2013**, *42*, 2388–2400, doi:10.1039/C2CS35272A.
136. Xiao, F.-X.; Hung, S.-F.; Miao, J.; Wang, H.-Y.; Yang, H.; Liu, B. Metal-Cluster-Decorated TiO 2 Nanotube Arrays: A Composite Heterostructure toward Versatile Photocatalytic and Photoelectrochemical Applications. *Small* **2015**, *11*, 554–567, doi:10.1002/smll.201401919.
137. Kurashige, W.; Kumazawa, R.; Mori, Y. Au25 Cluster-Loaded SrTiO3 Water-Splitting Photocatalyst; Preparation and Elucidation of the Effect of Cocatalyst Refinement on Photocatalytic Activity. *J. Mater. Appl.*
138. Attia, Y.A.; Buceta, D.; Blanco-Varela, C.; Mohamed, M.B.; Barone, G.; López-Quintela, M.A. Structure-Directing and High-Efficiency Photocatalytic Hydrogen Production by Ag Clusters. *J. Am. Chem. Soc.* **2014**, *136*, 1182–1185, doi:10.1021/ja410451m.
139. Shen, P.; Zhao, S.; Su, D.; Li, Y.; Orlov, A. Outstanding Activity of Sub-Nm Au Clusters for Photocatalytic Hydrogen Production. *Applied Catalysis B: Environmental* **2012**, *126*, 153–160, doi:10.1016/j.apcatb.2012.07.021.
140. Wang, H.; Luo, S.; Song, Y.; Shi, Y.; Wang, Z.; Guo, B.; Wu, L. Enhanced Photocatalytic Hydrogen Evolution over Monolayer HTi2NbO7 Nanosheets with Highly Dispersed Pt Nanoclusters. *Applied Surface Science* **2020**, *511*, 145501, doi:10.1016/j.apsusc.2020.145501.
141. Naveen, M.H.; Khan, R.; Bang, J.H. Gold Nanoclusters as Electrocatalysts: Atomic Level Understanding from Fundamentals to Applications. *Chem. Mater.* **2021**, *33*, 7595–7612, doi:10.1021/acs.chemmater.1c02112.
142. Du, X.L.; Wang, X.L.; Li, Y.H.; Wang, Y.L.; Zhao, J.J.; Fang, L.J.; Zheng, L.R.; Tong, H.; Yang, H.G. Isolation of Single Pt Atoms in a Silver Cluster: Forming Highly Efficient Silver-Based Cocatalysts for Photocatalytic Hydrogen Evolution. *Chem. Commun.* **2017**, *53*, 9402–9405, doi:10.1039/C7CC04061J.
143. Miyauchi, M.; Irie, H.; Liu, M.; Qiu, X.; Yu, H.; Sunada, K.; Hashimoto, K. Visible-Light-Sensitive Photocatalysts: Nanocluster-Grafted Titanium Dioxide for Indoor Environmental Remediation. *J. Phys. Chem. Lett.* **2016**, *7*, 75–84, doi:10.1021/acs.jpclett.5b02041.
144. Yin, G.; Nishikawa, M.; Nosaka, Y.; Srinivasan, N.; Atarashi, D.; Sakai, E.; Miyauchi, M. Photocatalytic Carbon Dioxide Reduction by Copper Oxide Nanocluster-Grafted Niobate Nanosheets. *ACS Nano* **2015**, *9*, 2111–2119, doi:10.1021/nn507429e.
145. Sagadevan, A.; Ghosh, A.; Maity, P.; Mohammed, O.F.; Bakr, O.M.; Rueping, M. Visible-Light Copper Nanocluster Catalysis for the C–N Coupling of Aryl Chlorides at Room Temperature. *J. Am. Chem. Soc.* **2022**, *144*, 12052–12061, doi:10.1021/jacs.2c02218.

146. Negishi, Y.; Mizuno, M.; Hirayama, M.; Omatoi, M.; Takayama, T.; Iwase, A.; Kudo, A. Enhanced Photocatalytic Water Splitting by BaLa4Ti4O15 Loaded with ~1 Nm Gold Nanoclusters Using Glutathione-Protected Au25 Clusters. *Nanoscale* **2013**, *5*, 7188, doi:10.1039/c3nr01888a.
147. Mousavi, H.; Small, T.D.; Sharma, S.K.; Golovko, V.B.; Shearer, C.J.; Metha, G.F. Graphene Bridge for Photocatalytic Hydrogen Evolution with Gold Nanocluster Co-Catalysts. *Nanomaterials* **2022**, *12*, 3638, doi:10.3390/nano12203638.
148. Schweinberger, F.F.; Berr, M.J.; Döblinger, M.; Wolff, C.; Sanwald, K.E.; Crampton, A.S.; Ridge, C.J.; Jäckel, F.; Feldmann, J.; Tschurl, M.; et al. Cluster Size Effects in the Photocatalytic Hydrogen Evolution Reaction. *J. Am. Chem. Soc.* **2013**, *135*, 13262–13265, doi:10.1021/ja406070q.
149. Kurashige, W.; Hayashi, R.; Wakamatsu, K.; Kataoka, Y.; Hossain, S.; Iwase, A.; Kudo, A.; Yamazoe, S.; Negishi, Y. Atomic-Level Understanding of the Effect of Heteroatom Doping of the Cocatalyst on Water-Splitting Activity in AuPd or AuPt Alloy Cluster-Loaded $BaLa_4Ti_4O_{15}$. *ACS Appl. Energy Mater.* **2019**, *2*, 4175–4187, doi:10.1021/acsaem.9b00426.
150. Méndez-Medrano, M.G.; Kowalska, E.; Lehoux, A.; Herissan, A.; Ohtani, B.; Rau, S.; Colbeau-Justin, C.; Rodríguez-López, J.L.; Remita, H. Surface Modification of TiO_2 with Au Nanoclusters for Efficient Water Treatment and Hydrogen Generation under Visible Light. *J. Phys. Chem. C* **2016**, *120*, 25010–25022, doi:10.1021/acs.jpcc.6b06854.
151. Tawalbeh, M.; Al-Othman, A.; Kafiah, F.; Abdelsalam, E.; Almomani, F.; Alkasrawi, M. Environmental Impacts of Solar Photovoltaic Systems: A Critical Review of Recent Progress and Future Outlook. *Science of The Total Environment* **2021**, *759*, 143528, doi:10.1016/j.scitotenv.2020.143528.
152. Kondratenko, E.V.; Mul, G.; Baltrusaitis, J.; Larrazábal, G.O.; Pérez-Ramírez, J. Status and Perspectives of CO2 Conversion into Fuels and Chemicals by Catalytic, Photocatalytic and Electrocatalytic Processes. *Energy Environ. Sci.* **2013**, *6*, 3112, doi:10.1039/c3ee41272e.
153. Roy, S.C.; Varghese, O.K.; Paulose, M.; Grimes, C.A. Toward Solar Fuels: Photocatalytic Conversion of Carbon Dioxide to Hydrocarbons. *ACS Nano* **2010**, *4*, 1259–1278, doi:10.1021/nn9015423.
154. Alper, E.; Yuksel Orhan, O. CO2 Utilization: Developments in Conversion Processes. *Petroleum* **2017**, *3*, 109–126, doi:10.1016/j.petlm.2016.11.003.
155. Du, C.; Wang, X.; Chen, W.; Feng, S.; Wen, J.; Wu, Y.A. CO2 Transformation to Multicarbon Products by Photocatalysis and Electrocatalysis. *Materials Today Advances* **2020**, *6*, 100071, doi:10.1016/j.mtadv.2020.100071.
156. Halmann, M. Photoelectrochemical Reduction of Aqueous Carbon Dioxide on P-Type Gallium Phosphide in Liquid Junction Solar Cells. *Nature* **1978**, *275*, 115–116, doi:10.1038/275115a0.
157. Olah, G.A. Beyond Oil and Gas: The Methanol Economy. *Angew. Chem. Int. Ed.* **2005**, *44*, 2636–2639, doi:10.1002/anie.200462121.
158. Lu, Q.; Jiao, F. Electrochemical CO2 Reduction: Electrocatalyst, Reaction Mechanism, and Process Engineering. *Nano Energy* **2016**, *29*, 439–456, doi:10.1016/j.nanoen.2016.04.009.
159. Philip Colombo, D.; Roussel, K.A.; Saeh, J.; Skinner, D.E.; Cavaleri, J.J.; Bowman, R.M. Femtosecond Study of the Intensity Dependence of Electron-Hole Dynamics in TiO2 Nanoclusters. *Chemical Physics Letters* **1995**, *232*, 207–214, doi:10.1016/0009-2614(94)01343-T.
160. Kauffman, D.R.; Alfonso, D.; Matranga, C.; Qian, H.; Jin, R. Experimental and Computational Investigation of Au_{25} Clusters and CO_2: A Unique Interaction and Enhanced Electrocatalytic Activity. *J. Am. Chem. Soc.* **2012**, *134*, 10237–10243, doi:10.1021/ja303259q.

161. Guo, S.-X.; MacFarlane, D.R.; Zhang, J. Bioinspired Electrocatalytic CO_2 Reduction by Bovine Serum Albumin-Capped Silver Nanoclusters Mediated by $[\alpha\text{-}SiW_{12}O_{40}]^{4-}$. *ChemSusChem* **2016**, *9*, 80–87, doi:10.1002/cssc.201501343.
162. Corma, A.; Garcia, H. Photocatalytic Reduction of CO2 for Fuel Production: Possibilities and Challenges. *Journal of Catalysis* **2013**, *308*, 168–175, doi:10.1016/j.jcat.2013.06.008.
163. Qin, L.; Ma, G.; Wang, L.; Tang, Z. Atomically Precise Metal Nanoclusters for (Photo)Electroreduction of CO2: Recent Advances, Challenges and Opportunities. *Journal of Energy Chemistry* **2021**, *57*, 359–370, doi:10.1016/j.jechem.2020.09.003.
164. Linsebigler, A.L.; Lu, G.; Yates, J.T. Photocatalysis on TiO2 Surfaces: Principles, Mechanisms, and Selected Results. *Chem. Rev.* **1995**, *95*, 735–758, doi:10.1021/cr00035a013.
165. Liu, M.; Qiu, X.; Miyauchi, M.; Hashimoto, K. Cu(II) Oxide Amorphous Nanoclusters Grafted Ti^{3+} Self-Doped TiO_2 : An Efficient Visible Light Photocatalyst. *Chem. Mater.* **2011**, *23*, 5282–5286, doi:10.1021/cm203025b.
166. Shoji, S.; Yin, G.; Nishikawa, M.; Atarashi, D.; Sakai, E.; Miyauchi, M. Photocatalytic Reduction of CO2 by Cu O Nanocluster Loaded SrTiO3 Nanorod Thin Film. *Chemical Physics Letters* **2016**, *658*, 309–314, doi:10.1016/j.cplett.2016.06.062.
167. Jin, J.; Luo, J.; Zan, L.; Peng, T. One-Pot Synthesis of Cu-Nanocluster-Decorated Brookite TiO_2 *Quasi* -Nanocubes for Enhanced Activity and Selectivity of CO_2 Photoreduction to CH_4. *ChemPhysChem* **2017**, *18*, 3230–3239, doi:10.1002/cphc.201700563.
168. Cui, X.; Wang, J.; Liu, B.; Ling, S.; Long, R.; Xiong, Y. Turning Au Nanoclusters Catalytically Active for Visible-Light-Driven CO_2 Reduction through Bridging Ligands. *J. Am. Chem. Soc.* **2018**, *140*, 16514–16520, doi:10.1021/jacs.8b06723.
169. Jiang, Y.; Yu, Y.; Zhang, X.; Weinert, M.; Song, X.; Ai, J.; Han, L.; Fei, H. N-Heterocyclic Carbene-Stabilized Ultrasmall Gold Nanoclusters in a Metal-Organic Framework for Photocatalytic CO_2 Reduction. *Angew. Chem. Int. Ed.* **2021**, *60*, 17388–17393, doi:10.1002/anie.202105420.
170. Billo, T.; Fu, F.-Y.; Raghunath, P.; Shown, I.; Chen, W.-F.; Lien, H.-T.; Shen, T.-H.; Lee, J.-F.; Chan, T.-S.; Huang, K.-Y.; et al. Ni-Nanocluster Modified Black TiO_2 with Dual Active Sites for Selective Photocatalytic CO_2 Reduction. *Small* **2018**, *14*, 1702928, doi:10.1002/smll.201702928.
171. Chen, Y.-S.; Kamat, P.V. Glutathione-Capped Gold Nanoclusters as Photosensitizers. Visible Light-Induced Hydrogen Generation in Neutral Water. *J. Am. Chem. Soc.* **2014**, *136*, 6075–6082, doi:10.1021/ja5017365.
172. Zhang, L.; Can, M.; Ragsdale, S.W.; Armstrong, F.A. Fast and Selective Photoreduction of CO_2 to CO Catalyzed by a Complex of Carbon Monoxide Dehydrogenase, TiO_2 , and Ag Nanoclusters. *ACS Catal.* **2018**, *8*, 2789–2795, doi:10.1021/acscatal.7b04308.
173. El-Roz, M.; Telegeiev, I.; Mordvinova, N.E.; Lebedev, O.I.; Barrier, N.; Behilil, A.; Zaarour, M.; Lakiss, L.; Valtchev, V. Uniform Generation of Sub-Nanometer Silver Clusters in Zeolite Cages Exhibiting High Photocatalytic Activity under Visible Light. *ACS Appl. Mater. Interfaces* **2018**, *10*, 28702–28708, doi:10.1021/acsami.8b09634.